Seismotectonics beneath the Tokyo metropolitan area, Japan: Effect of slab-slab contact and overlap on seismicity

Junichi Nakajima,[1] Fuyuki Hirose,[2] and Akira Hasegawa[1]

Received 17 September 2008; revised 6 April 2009; accepted 11 June 2009; published 28 August 2009.

[1] We first determine the configuration of the upper surface of the Pacific (PAC) slab beneath Kanto, Japan, from the distribution of interplate earthquakes relocated by an appropriate 1-D velocity model. Then, traveltime tomography is carried out to estimate three-dimensional seismic velocity structures around Kanto using 735,520 P wave and 444,049 S wave arrival times from 6508 local earthquakes. The obtained results suggest that the Philippine Sea (PHS) slab is subducting to depths of 130–140 km without a gap, even to the northwest of the Izu collision zone. We subsequently define the lateral extent of the contact zone between the bottom of the PHS slab and the upper surface of the PAC slab (PHS-PAC interface) and reveal that the slab contact zone underlies a wider area beneath Kanto in harmony with the Kanto plain. The downdip limit of interplate (thrust-type) earthquakes on the PAC slab is deepened by ~30 km locally under the slab contact zone. This deepening is probably caused by a lower-temperature environment in the PAC slab, resulting from the overlap with the PHS slab subducting above and consequent thermal shielding by the PHS slab from the hot mantle wedge. We detect an extremely low-velocity anomaly in the easternmost portion of the PHS slab, which is probably attributable to serpentinization of mantle peridotite. Interplate earthquakes are almost absent along the PHS-PAC interface overlain by the serpentinized mantle in the PHS slab, suggesting that ductile deformation takes place along the interface because of low viscosity of the serpentine.

Citation: Nakajima, J., F. Hirose, and A. Hasegawa (2009), Seismotectonics beneath the Tokyo metropolitan area, Japan: Effect of slab-slab contact and overlap on seismicity, *J. Geophys. Res.*, *114*, B08309, doi:10.1029/2008JB006101.

1. Introduction

[2] The Kanto district in central Japan, which surrounds the Tokyo metropolitan area, is known as a unique region in the world in terms of plate tectonics. This region is located behind a trench-trench-trench (TTT) triple junction with two obliquely subducting oceanic plates, the Philippine Sea (PHS) and Pacific (PAC) plates. The PHS plate subducts under the continental, Okhotsk (OKH) or North American, plate along the Sagami and Nankai troughs, and the PAC plate subducts below the PHS and continental plates along the Japan and Izu-Bonin trenches (Figure 1). The Izu-Bonin volcanic ridge, an island arc that was formed in an intra-oceanic setting, has been colliding with central Japan during 15 Ma at the western margin of the Kanto district, and the Izu peninsula is in collision at present [e.g., *Soh et al.*, 1998].

[3] Many disastrous M ~ 8 and numerous M ~ 7 earthquakes have struck the Tokyo metropolitan area. For example, the 1923 Kanto earthquake (M7.9), one of the most destructive earthquakes in the 20th century, caused severe damage to the Tokyo metropolitan area, along with 105,000 fatalities. This area now has a population of ~33 million, a fourth of Japan's population. The Japanese government estimates that a future M7 or greater earthquake will result in ~11,000 fatalities and economic damaging totaling up to 112 trillion yens (~1.1 trillion dollars) [*Central Disaster Management Council*, 2004], which exceeds the annual budget of the government. There is a 70% probability that such an earthquake will occur within the next 30 years (Earthquake Research Committee, Long-term evaluation of earthquakes along the Sagami trough (in Japanese, 2004, available at http://www.jishin.go.jp/main/chousa/04aug_sagami/index.htm).

[4] The configuration of the PHS slab in central Japan has been generated much interest, and various models have been proposed on the basis of hypocenter distributions, focal mechanisms, later phase analyses, three-dimensional (3-D) seismic velocity structures, and reflection/refraction surveys [e.g., *Iidaka et al.*, 1990; *Ishida*, 1992; *Sekiguchi*, 2001; *Kodaira et al.*, 2004; *Sato et al.*, 2005; *Matsubara et al.*, 2005; *Kimura et al.*, 2006; *Hori*, 2006; *Wu et al.*, 2007; *Nakajima and Hasegawa*, 2007]. Recently, *Hirose et al.* [2007, 2008a, 2008b] delineated, through careful investigation of 3-D seismic velocity structures and the distribution of interplate (thrust-type) earthquakes, the upper surface of the PHS slab at depths of <90 km in Kanto and <60 km in

[1]Research Center for Prediction of Earthquakes and Volcanic Eruptions, Graduate School of Science, Tohoku University, Sendai, Japan.
[2]Seismology and Volcanology Research Department, Meteorological Research Institute, Tsukuba, Japan.

Copyright 2009 by the American Geophysical Union.
0148-0227/09/2008JB006101$09.00

southwestern (SW) Japan. In spite of these extensive studies, however, the subduction of the PHS plate toward the northwest of the Izu peninsula is still in controversy (a slab gap in Figure 1b), preventing us from constructing the entire slab geometry of the PHS slab.

[5] South of the Sagami trough, where the PHS plate is not yet subducting, the PHS plate is in contact with the subducting PAC plate just west of the Izu-Bonin trench (Figure 1a). Since the relative plate motion between the PHS and PAC plates is almost E–W [*Seno et al.*, 1996], the contact between the two slabs can be kept even after the subduction. There are, therefore, three types of slab interface beneath Kanto (OKH-PAC, OKH-PHS, and PHS-PAC interfaces) (Figure 1c). The PHS-PAC interface, where the bottom of the PHS slab is in contact with the upper surface of the PAC slab, is a unique feature resulting from the subduction of the two slabs. The lateral extent of the PHS-PAC interface (hereafter referred to as the slab contact zone) has been partially defined in previous studies [e.g., *Huchon and Labaume*, 1989; *Seno and Takano*, 1989; *Okada and Kasahara*, 1990; *Wu et al.*, 2007; *Hasegawa et al.*, 2007; *Uchida et al.*, 2009], and the seismotectonics beneath Kanto have been debated in relation to slab-slab contact. In particular, *Wu et al.* [2007] discussed the seismicity beneath Kanto in detail, in terms of the interaction between the two slabs, and suggested the important role of slab-slab interaction in the seismic hazard under the Tokyo metropolitan area.

[6] This paper describes the seismotectonics beneath Kanto with a consideration of the interactions between two oceanic plates and a continental plate. In the following sections, we first estimate the detailed 3-D seismic velocity structures of the crust and the uppermost mantle, which incorporates the determination of the upper surfaces of the PAC and PHS slabs and the lateral extent of the slab contact zone. Then, we discuss the occurrence of interplate earthquakes along the upper surface of the two slabs, in terms of lower-temperature environments because of the slab-slab contact and serpentinized mantle in the easternmost portion of the PHS slab.

2. Slab Geometry, 3-D Seismic Velocity Structure, and Slab Contact Zone

[7] This section gives a step-by-step description of the method used to estimate the geometry of the two slabs, 3-D seismic velocity structures, and slab contact zone beneath Kanto. The following is a summary of our strategy.

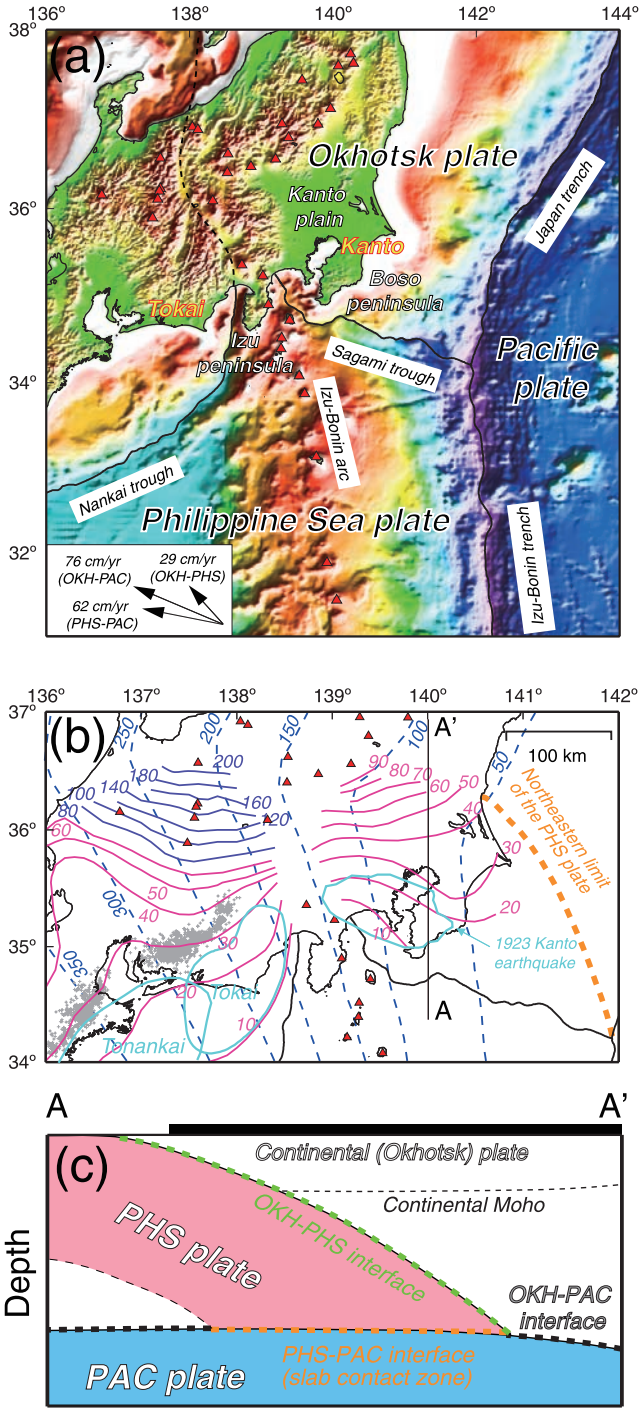

Figure 1. (a) Tectonic settings in the study area. Red triangles denote active volcanoes. Relative plate motions between the Pacific (PAC) and Philippine Sea (PHS) plates, the PAC and Okhotsk (OKH) plates, and the PHS and OKH plates [*Seno et al.*, 1993, 1996] are shown by arrows in the box. (b) The isodepth contours of the PHS slab estimated by *Nakajima and Hasegawa* [2007] and *Hirose et al.* [2007, 2008a, 2008b] are shown by purple and pink lines, respectively, and those of the PAC slab estimated by *Nakajima and Hasegawa* [2006] are shown by blue dashed lines. Gray crosses denote nonvolcanic deep tremors [*Obara*, 2002]. The northeastern limit of the PHS slab estimated by *Uchida et al.* [2009] is shown by an orange dashed line. Source areas of the 1923 Kanto earthquake (M7.9) [*Wald and Somerville*, 1995] and the Tokai and Tonankai earthquakes (Headquarters for Earthquake Research Promotion, On the long-term evaluation of earthquakes in the Nankai Trough (in Japanese), 2001, available at http://www.jishin.go.jp/main/chousa/01sep_nankai/index.htm) are enclosed by light blue lines. (c) A schematic representation (not scaled) of three types of slab interfaces along line A-A′ in Figure 1b. A black bar on the top denotes the land area.

[8] Step A: An appropriate one-dimensional (1-D) seismic velocity model and station corrections are estimated using the VELEST inversion. Then, earthquakes are relocated using the obtained velocity model.

[9] Step B: The upper surface of the PAC slab is defined from the distribution of interplate earthquakes relocated with the 1-D model estimated in step A. In this step, we regard earthquakes with focal mechanisms of 135° < strike < 225°, 0° < dip < 30°, and 45° < rake < 135° as interplate (low-angle thrust-type) earthquakes along the PHS-PAC interface, based on the plate model by *Seno et al.* [1993, 1996].

[10] Step C: Traveltime tomography is carried out to estimate 3-D seismic velocity structures, taking into account the geometry of the PAC slab obtained in step B. Then, earthquakes are relocated using the final 3-D velocity model.

[11] Step D: The upper surface of the PHS slab is delineated at the northwest extension of the Izu collision zone on the basis of 3-D seismic velocity structures obtained in Step C.

[12] Step E: The lateral extent of the slab contact zone is estimated from the newly determined geometries of the two slabs in steps B and D.

2.1. Earthquake Relocation Using 1-D Velocity Model, Step A

[13] Since October 1997 the Japan Meteorological Agency (JMA) has processed the data from seismograph stations throughout the Japanese Islands to produce a comprehensive seismic catalog for Japan (JMA unified catalog). However, this catalog has two disadvantages; the neglect of station elevations and the lack of consideration of station corrections for OBS stations [*Harada*, 2004] (see Appendix A for details). Therefore, we first estimated an appropriate 1-D velocity model and station corrections using the VELEST inversion [*Kissling et al.*, 1994] to obtain precise hypocenter locations beneath Kanto. In the inversion, arrival time data from 658 earthquakes in the JMA unified catalog were inverted using an initial velocity model derived from a stratified JMA2001 model [*Ueno et al.*, 2002], and the final 1-D velocity model and station corrections were obtained (Figures A1 and A2). We then relocated 64,984 earthquakes (M > 1.0) that occurred during 2001–2007 at latitudes in the range of 32–37°N, longitudes in the range of 138–142°E, and depths in the range of 0–400 km using the final 1-D velocity model and station corrections. The errors for the relocated hypocenters were generally less than ~1 km in the horizontal direction and ~2 km in the vertical direction. Figure 2 shows a comparison between the relocated hypocenters and original ones determined by the JMA. Beneath the land area, the earthquakes of the JMA at depths of 40–80 km became 5–10 km deeper, whereas those at greater depths became ~5 km deeper with westward shifts of ~5 km (Figure 2b). In offshore regions, the hypocenters generally became 5–10 km deeper, with northward shifts of 5–10 km (Figure 2c). The scattered shifts of the hypocenters for earthquakes that occurred far from the land area may be due to the lack of accuracy in relocating the earthquakes.

2.2. Delineation of the Upper Surface of the PAC Slab, Step B

[14] Figure 3 shows six E–W vertical cross sections of relocated hypocenters and focal mechanisms of interplate earthquakes for nine prominent clusters along the PHS-PAC interface. Focal mechanism solutions for 258 small earthquakes (1 < M < 3) around the upper surface of the PAC slab that are not included in the JMA unified catalog were determined manually by reading initial P wave polarities from raw records. Earthquakes in the nine clusters have low-angle thrust-type focal mechanisms whose strike and slip vectors are consistent with relative plate motion along the PHS-PAC interface [*Seno et al.*, 1993, 1996]. We thus delineated the upper surface of the PAC slab passing through the interplate earthquake clusters at depths of <80 km. At depths of >80 km where interplate earthquakes have not been observed, we determined the upper surface of the PAC slab along the upper envelope of relocated intermediate-depth earthquakes. This methodology can be supported by the recent observations that most intraslab earthquakes in the upper plane of the double-seismic zone occur in the oceanic crust at depths of 60–150 km [*Kita et al.*, 2006; *Hasegawa et al.*, 2007; *Tsuji et al.*, 2008; *Nakajima et al.*, 2009]. At depths of >150 km, where seismic activity is not very high and earthquakes in the upper and lower planes of the double seismic zone tend to merge, the upper surface of the PAC slab was estimated so as to connect smoothly with that at shallower depths. The uncertainties in the upper surface of the PAC slab at depths of <150 km were ~2 km in the vertical direction, mainly resulting from errors in hypocenter locations, whereas those at depths of >150 km may be 4–5 km due to the ambiguity of the delineation of the slab surface in addition to hypocenter errors. Nineteen E–W vertical cross sections were constructed in total, and the upper surface of the PAC slab was determined in each cross section in the same manner.

[15] Figure 4 shows a comparison of the upper surface of the PAC slab determined in this study with those determined in the previous models. The overall configurations are similar, and all of the models have a single cusp at the latitude of ~36°N corresponding to a change in the strike of the trench. Compared to the most recent model by *Nakajima and Hasegawa* [2006], who estimated the slab surface from the earthquakes in the JMA unified catalog, the present model becomes deeper beneath the central part of Kanto and shows a smoother curvature of the cusp. These discrepancies can be due to the shifts in the hypocenters beneath the land area to greater depths after the relocation (A-A′ in Figure 2), and possibly to wrong identification of earthquakes in the PHS slab as occurring in the PAC slab in the work by *Nakajima and Hasegawa* [2006]. The present model almost coincides with that by *Ishida* [1992] at depths of 60–100 km and with that by *Ohmi and Hori* [2000] at depths of 80–100 km.

2.3. Three-Dimensional Seismic Velocity Structures, Step C

[16] Tomographic method of *Zhao et al.* [1992a] was applied to 735,520 P and 444,049 S wave arrival time data from 6508 earthquakes recorded at 637 seismograph stations (Figure 5) in order to determine 3-D P and S wave

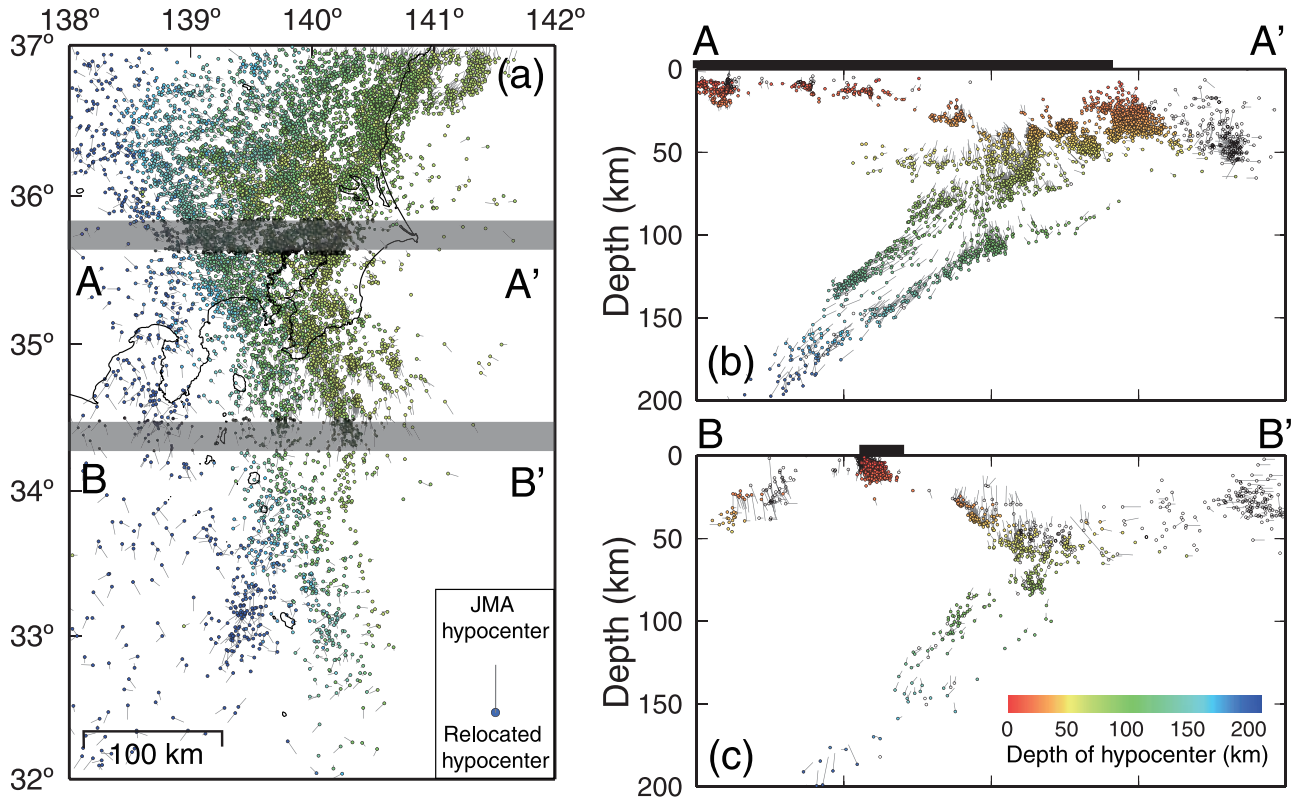

Figure 2. (a) Comparison between the original JMA locations and those relocated with the final 1-D velocity model determined by the VELEST inversions. Relocated hypocenters are plotted by colored scaled to focal depths. Only earthquakes with depths of >60 km are shown. (b) E–W vertical cross section along A-A′ in Figure 2a. (c) E–W vertical cross section along B-B′ in Figure 2a. Black bar on the top represents the land area. Open circles denote earthquakes that do not satisfy the following criterion: $H^{dep} > D^{min}$, where H^{dep} is a depth of an earthquake and D^{min} is an epicentral distance to the nearest station with pickings of P or S wave arrival times.

velocity structures. The final 1-D velocity model obtained by the VELEST inversions was adopted as an initial model (red curve in Figure A1). The crustal discontinuities (the Conrad and Moho) estimated by *Zhao et al.* [1992b] and the upper surface of the PAC slab determined in this study were taken into account and fixed during the inversion. Grid nodes with a spacing of 0.15°–0.2° in the latitude and 0.2° in the longitude directions were set in the model space. Grid nodes were spaced vertically at 5–20 km for depths of <180 km and 30–40 km for greater depths (Figure B1). The final results were obtained after five iterations. The RMS values of traveltime residuals, which were 0.35 s for the P wave and 0.59 s for the S wave for the initial model, were reduced to 0.21 s and 0.43 s, respectively. A detailed description of the method of tomographic inversions, uncertainties in the obtained velocity models, and results of the resolution tests is summarized in Appendix B.

[17] Figure 6 depicts a map showing P and S wave velocity structures to a depth of 210 km. Here we focus on heterogeneous structures related to the subduction of the PHS and PAC slabs. A characteristic E–W trending low-velocity zone (pink arrows) exists beneath Kanto at depths of 25 and 40 km, which has been interpreted to be the crust of the PHS slab [e.g., *Ohmi and Hurukawa*, 1996; *Sekiguchi*, 2001], serpentinized mantle wedge in the overlying continental plate [*Kamiya and Kobayashi*, 2000; *Matsubara et al.*, 2005], or lower crustal materials dragged downward by the tectonic erosion of the continental plate due to the

Figure 3. (a) E–W vertical cross sections of hypocenters relocated with the final 1-D velocity model along six lines in the map. Black crosses denote earthquakes that satisfy the following criterion: $H^{dep} > D^{min}$ (see Figure 2), while gray ones denote earthquakes that do not satisfy this criterion. Red stars denote interplate earthquakes with low-angle thrust-type focal mechanisms along the upper surface of the PAC slab. Blue lines represent the upper surface of the PAC slab delineated in this study. The estimated isodepth contours of the PAC slab with an interval of 20 km, together with the distribution of interplate earthquakes (red stars), are shown in the map. (b) Fault plane solutions with P and T axes in a lower hemisphere equal-area projection for the earthquakes in the nine clusters in Figure 3a. Blue curve in each beach ball represents the local dip and strike of the PAC slab.

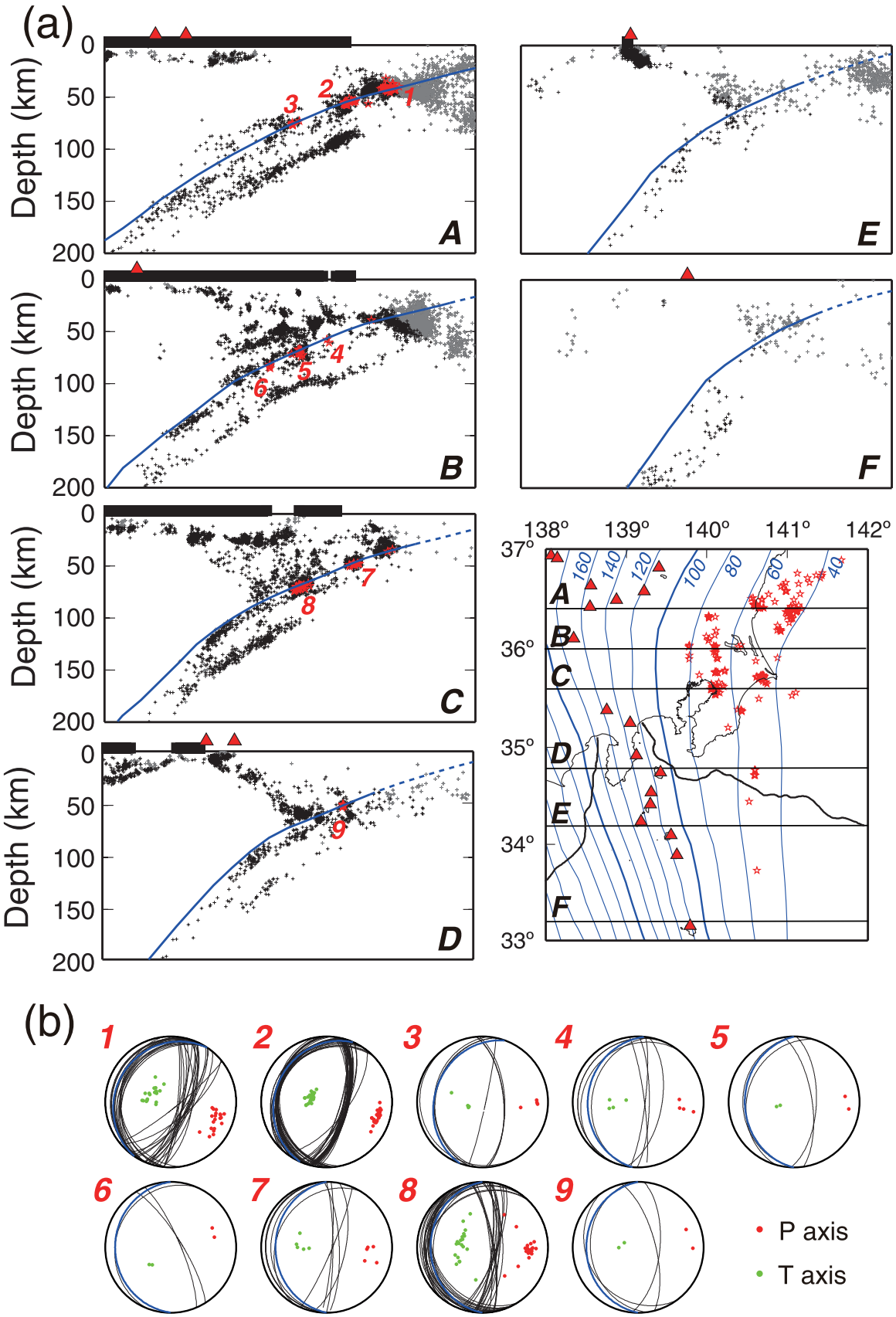
(a)
Depth (km)
0
50
100
150
200
A
B
C
D
E
F
1
2
3
4
5
6
7
8
9
138°
139°
140°
141°
142°
37°
36°
35°
34°
33°
160
140
120
100
80
60
40
(b)
P axis
T axis

Figure 3

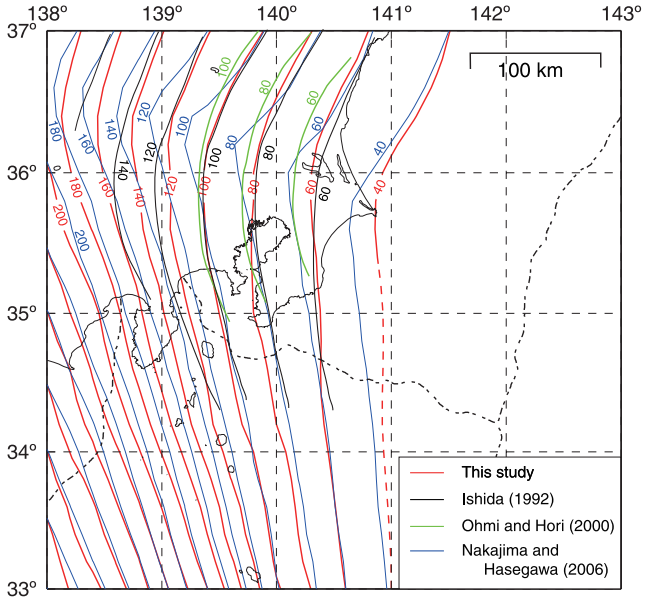

Figure 4. Map showing isodepth contours of the PAC slab estimated in this study (red lines) and in previous studies (black, green, and blue lines). The uncertainties in the lateral positions of the isodepth contours of the PAC slab because of location errors for relocated earthquakes are estimated to be ~10 km.

subduction of the PHS slab [*Wu et al.*, 2007]. An S wave low-velocity anomaly subparallel to the volcanic front is imaged in the back-arc side of northeastern (NE) Japan at depths of 40–140 km, which gradually shifts to the west with increasing depths. This low-velocity anomaly is considered to correspond to mantle upwelling flow induced by the subduction of the PAC slab [e.g., *Nakajima et al.*, 2001; *Hasegawa and Nakajima*, 2004]. High-velocity anomalies distributed roughly in the E–W direction are observed at the latitudes of 35–36.5°N, in particular in S waves, in a depth range of 60–120 km (white arrows at each depth). Since these anomalies appear to shift to the north with depth, we interpret them as the subducting PHS slab, as discussed in 2.4 in detail. These high-velocity anomalies can be traced continuously down to a depth of ~140 km.

[18] In order to discuss the seismic activity related to the subduction of the two slabs beneath Kanto, we relocated 95,879 earthquakes that occurred during 2001–2007 in the latitude range of 34–38°N, longitude range of 136–142°E, and depth range of 0–400 km using the final 3-D velocity model obtained by the tomographic inversions. The relocated hypocenters are hereafter shown and used for discussion. Average errors in the locations of relocated earthquakes were estimated to be ~1 km and ~2 km in the horizontal and vertical directions, respectively.

2.4. Configuration of the PHS Slab, Step D

[19] On the basis of the obtained 3-D seismic velocity structure, we determined the upper surface of the PHS slab toward the northwest of the Izu peninsula under two assumptions. One is that intermediate-depth earthquakes only occur in subducting slabs. The other is that the crust of the PHS slab shows a lower seismic velocity than the mantle in the overlying continental plate at depths of <60 km because of the presence of hydrous minerals, and both the crust and mantle of the PHS slab show higher seismic velocity than the overlying mantle wedge at greater depths because hydrous minerals in the oceanic crust can be transformed into eclogite [e.g., *Hacker et al.*, 2003]. In the delineation, the upper surface of the PHS slab proposed by *Hirose et al.* [2007, 2008a, 2008b] is fixed (gray lines in Figure 7) because they determined it precisely by referring to the distribution of interplate earthquakes relocated with 3-D velocity models and a low-velocity layer interpreted as oceanic crust.

[20] Figure 7 shows that prominent high-velocity anomalies are distributed at depths of 70–120 km beneath the westernmost part of Kanto, which are labeled as Q, P, and O, in lines A, B, and C, respectively. In line C, the upper surface of the PHS slab determined by *Hirose et al.* [2008a] (gray lines) runs above the eastern half of this high-velocity anomaly. Since an earthquake interpreted as an interplate earthquake along the upper surface of the PHS slab (a white circle in Figure 7c) [*Matsubara et al.*, 2008] occurred at the westward extension of the slab surface determined by *Hirose et al.* [2008a], we extended the slab surface smoothly to the Tokai district through this earthquake. We interpret the high-velocity anomalies, Q and P, to be the PHS slab as

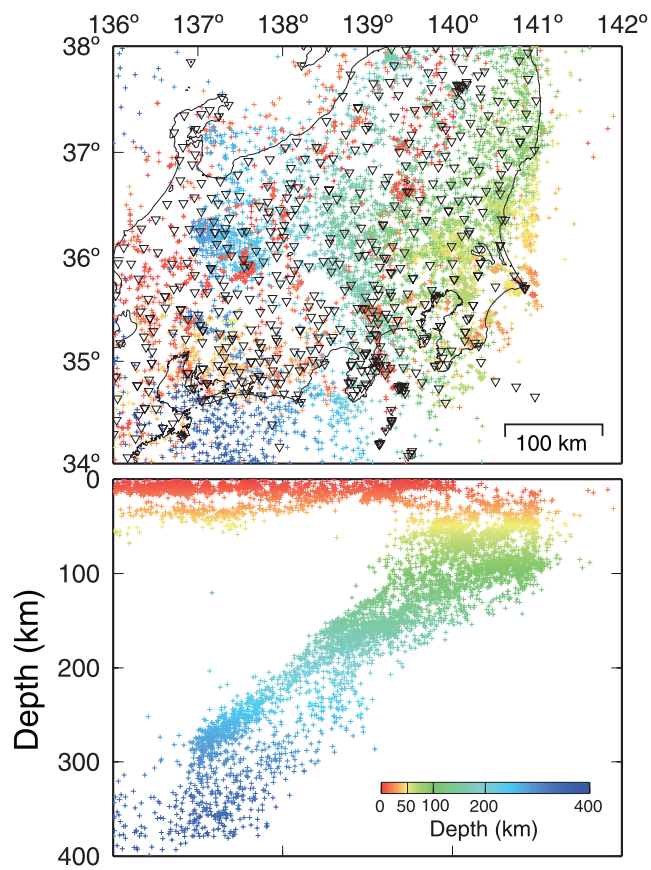

Figure 5. Distribution of 6508 earthquakes (colored crosses) and 637 seismograph stations (reverse triangles) used in this study. Colors represent the hypocenter depths.

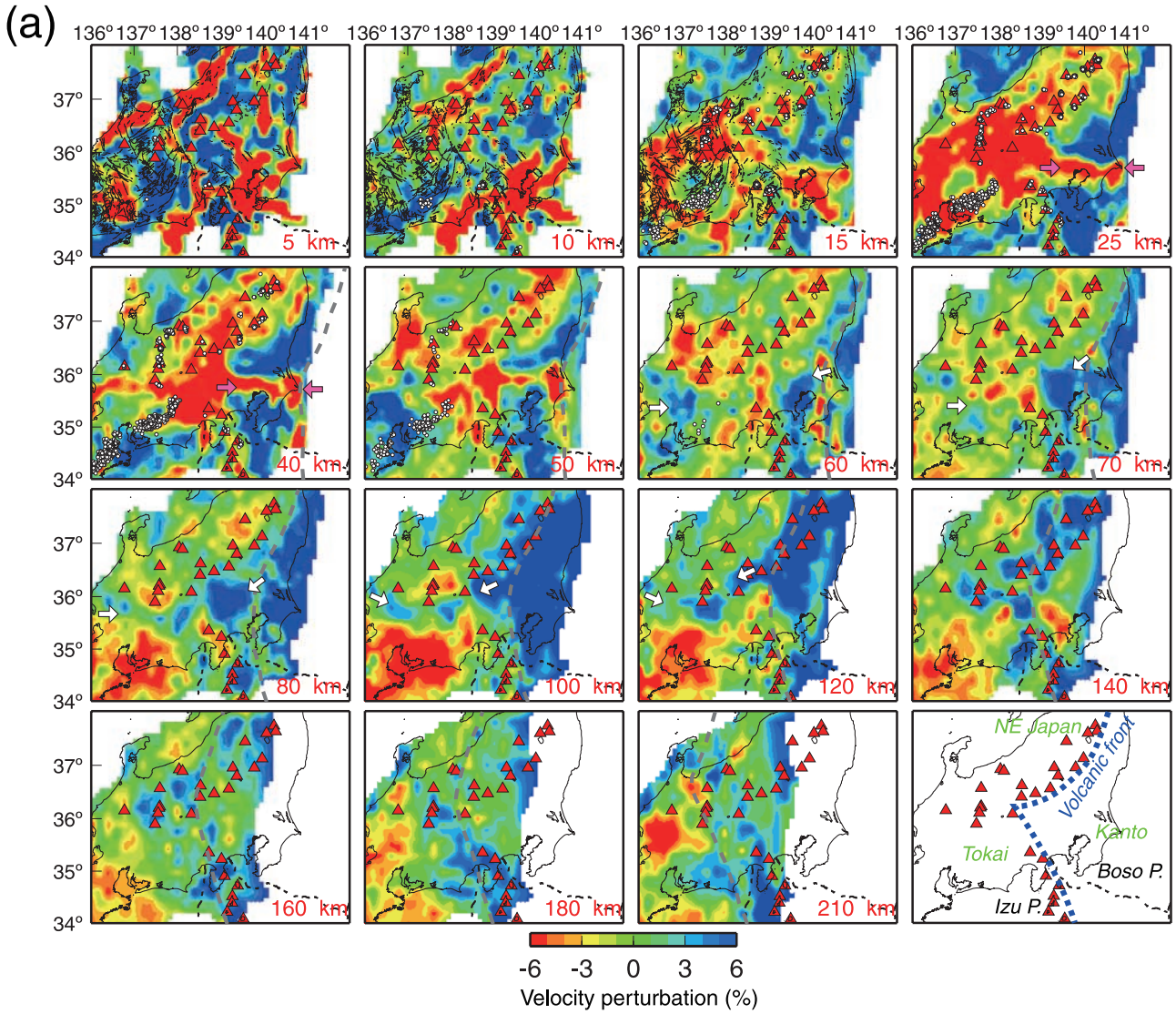

Figure 6. Distribution of (a) P and (b) S wave velocity perturbations (in %). The velocity perturbations shown are the deviations from the average velocities at each depth. Red triangles represent active volcanoes. Active faults are plotted on the velocity images at depths of 5–15 km by black lines. White circles represent deep low-frequency earthquakes reported by the JMA. The regions with a number of rays >1000 are shown. Gray dashed curves shown at depths of 40–210 km represent the upper surface of the PAC slab. The characteristic velocity anomalies discussed in the text are shown by pink arrows at depths of 25 and 40 km and white arrows at depths of 60–120 km. The bottom right plot represents the names of the regions discussed in the text.

well, and the upper surface of the PHS slab is determined to be immediately above these anomalies in lines A and B. An important point to be noticed is the existence of continuous high-velocity anomalies at the northwest extension of the Izu collision zone in lines A–C, even though the amplitude of these high-velocity anomalies appears to be weak. These observations suggest that the PHS slab is subducting to a depth of ~140 km without a gap, even to the northwest of the Izu collision zone (pink dashed lines in Figure 7). This implies that the previous interpretation by *Nakajima and Hasegawa* [2007] (gray dashed lines in Figures 7a–7c) may be wrong.

[21] The isodepth contours of the newly determined upper surface of the PHS slab incorporated with those by *Hirose et al.* [2007, 2008a, 2008b] are shown in Figure 8, together with previous models. The strike of the isodepth contours in our model is in agreement with that by *Hori* [2006] at depths of >40 km even though the slab depth estimated by *Hori* [2006] is slightly shallower than in our model. A southward concave of the isodepth contour of the slab at depths of 20–30 km is seen beneath the Boso peninsula, as indicated by *Ishida* [1992]. The dip of the upper surface estimated by *Iidaka et al.* [1990] is steeper at depths shallower than 30 km.

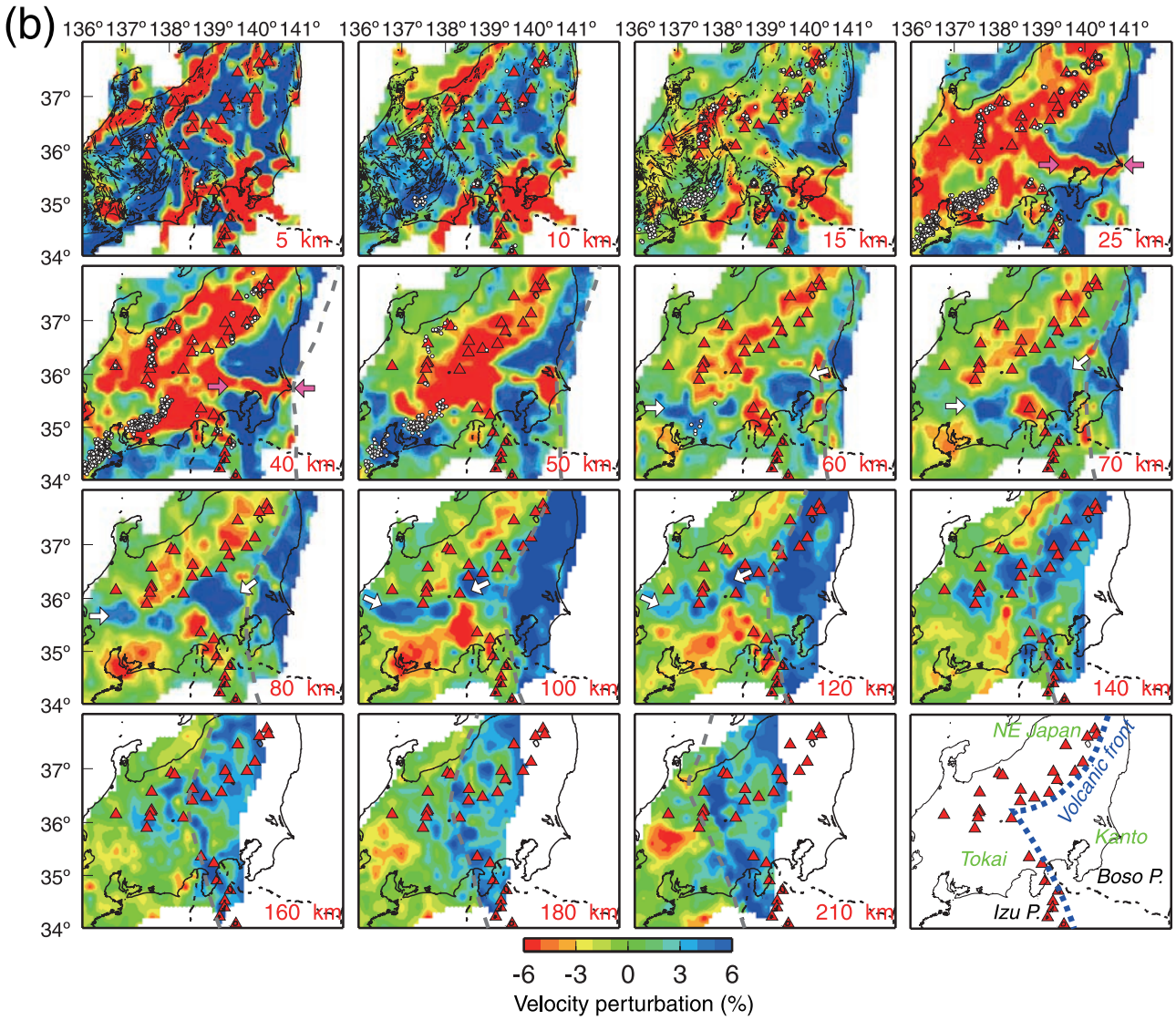

Figure 6. (continued)

Figure 7. Along-arc vertical cross sections of (left) P and (right) S wave velocity perturbations along profiles (a) A, (b) B, (c) C, (d) D, and (e) E. Locations are shown in the inset map. Pink lines indicate the upper surface of the PHS slab determined in this study. Note that pink dashed lines denote the slab surface where its location is not constrained by the distribution of a high-velocity anomaly. Gray solid and dashed lines represent the upper surface of the PHS slab previously estimated by *Hirose et al.* [2007, 2008a, 2008b] and *Nakajima and Hasegawa* [2007], respectively. The approximate locations of the bottom of the PHS slab are shown by black dashed lines. The upper surface of the PAC slab estimated in this study is shown by black lines. Orange dashed lines indicate the slab contact zone (PHS-PAC interface). Orange inverted triangles at the tops of Figures 7d and 7e represent the northeastern limit of the PHS slab estimated by *Uchida et al.* [2009], which is also shown in the inset map by an orange dashed line. Green ticks at the top of each plot and a green shaded area in the insert map show the schematic locations of the northwestward extension of the Izu collision zone. The earthquakes relocated with 3-D seismic velocity structures are shown by crosses. White circles and squares denote interplate earthquakes and small repeating earthquakes [*Uchida et al.*, 2009], respectively, along the upper surfaces of the PAC and PHS slabs, which are also relocated with the 3-D seismic velocity structures. The labels, O, P, and Q, denote the high-velocity anomalies discussed in the text. A white circle with a white arrow in Figure 7c represents an interplate earthquake (M3.1) that occurred in 2006 [see *Matsubara et al.*, 2008]. The focal mechanism of this event is shown in Figure 7c in the lower hemisphere equal-area projection. A gray arrow in Figure 7e denotes the inclined seismicity toward the east discussed in the text, and white dashed circles in Figures 7d and 7e indicate the possible gap of the two slabs discussed in the text.

2.5. Lateral Extent of Contact Zone Between the PHS and PAC Slabs, Step E

[22] To determine the lateral extent of the slab contact zone (PHS-PAC interface) beneath Kanto, we need to constrain its northeastern (updip) and southwestern (downdip) limits. The northeastern (updip) limit of the slab contact zone, which corresponds to that of the PHS slab, has been estimated by the slip vectors of interplate earthquakes [*Seno and Takano*, 1989; *Noguchi*, 2007]. Recently, *Uchida et al.* [2009] investigated the focal mechanism solutions of interplate earthquakes that occurred along the PHS-PAC and OKH-PAC interfaces, and determined the northeastern limit of the PHS slab off the Boso peninsula (orange triangles in Figures 7d and 7e). Therefore, the upper surface of the PHS slab was also extended smoothly to the northeastern limit estimated by *Uchida et al.* [2009], as shown by pink lines in Figure 7. Interestingly, there may be a gap of 5–10 km between the depths of the PHS and PAC slabs around the northeastern limit (white dashed circle in Figures 7d and 7e). This gap suggests that the tip of the PHS slab is eroded by the subduction of the PAC slab immediately below it and partly accumulated around the northeastern limit of the PHS slab.

[23] *Kamiya and Kobayashi* [2007] pointed out that an eastward inclined seismicity that extends from the southern part of Kanto to the zone of the Sagami trough (gray arrow

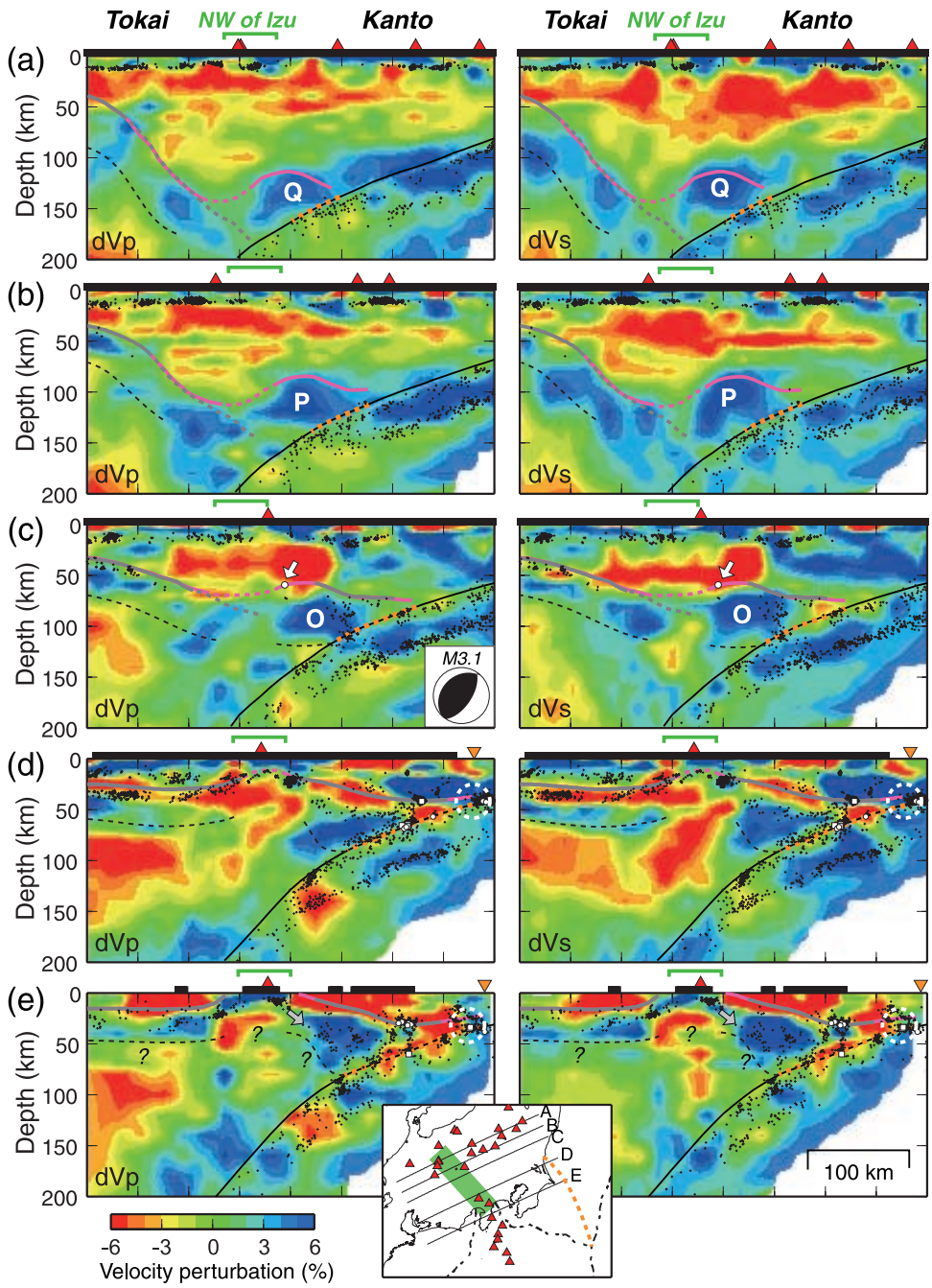

Figure 7

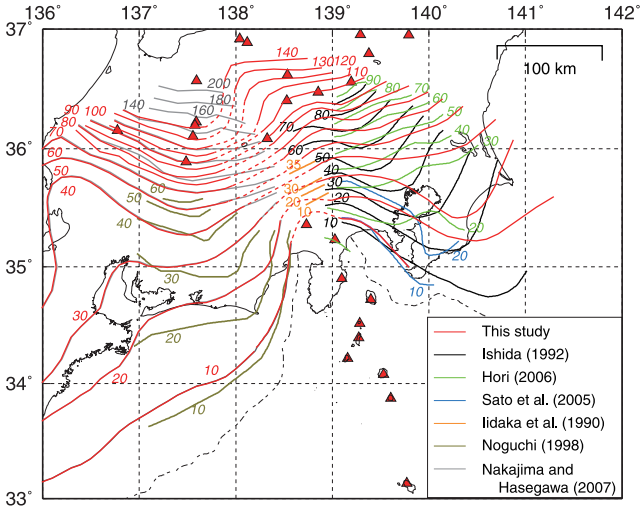

Figure 8. Map showing the isodepth contours of the PHS slab estimated in this study (red line) and in previous studies (black, green, blue, orange, gold, and gray lines).

in Figure 7e) occurs in the mantle of the PHS slab with high-velocity anomaly, and suggested that the thickness of the PHS slab is about 60 km beneath Kanto. Since our results also show that these earthquakes take place in a high-velocity anomaly with a vertical thickness of ~60 km, we infer the high-velocity anomaly accompanied by inclined seismicity to be the subducting PHS slab. The bottom of the PHS slab was estimated on the basis of the thickness of the high-velocity anomaly and seismicity, which enables us to define the slab contact zone as shown in Figure 7.

[24] The lateral extent of the slab contact zone thus estimated is shown in Figure 9. The southwestern limit of the slab contact zone beneath the land area agrees well with that proposed by *Noguchi* [2007] and *Hasegawa et al.* [2007]. South of the Sagami trough, we simply assumed that the thickness of the PHS slab is 60 km and defined the southwestern limit of the contact zone. If the thickness of the PHS slab is assumed to be ~70 km [*Pacanovsky et al.*, 1999], the western limit is shifted to the west by 15–20 km. The thickness of the PHS slab varies drastically from the northeastern to the southwestern limits of the slab contact zone. Interestingly, there appears to be a correlation between the lateral extent of the slab contact zone and that of the Kanto plain, the largest plain in Japan. Although further discussion on a geological timescale is required to relate the lateral extent of the slab contact zone to the formation of the Kanto plain, this result implies that slab-slab contact plays an important role in the subsidence of the Kanto plain.

3. Slab Dehydration, Serpentinization, Seismicity, and Interplate Coupling

[25] Before describing the tectonic implications of our results, we briefly review the subduction zone process expected beneath Kanto in terms of slab dehydration, the resultant metamorphic reaction, and its effect on the interplate coupling.

[26] The subduction of oceanic plates at the trench carries water into the earth in the form of hydrous minerals. The subducting oceanic crust consists of a relatively thin heterogeneous layer of marine sediments, an upper 2–3 km thick sequence of layered hydrothermally altered basalts, and a less altered lower portion composed mainly of gabbroic rocks, with an average composition similar to the basaltic portion [e.g., *Alt*, 1995]. The hydrous minerals in the oceanic crust become unstable with increasing pressures and temperatures [e.g., *Schmidt and Poli*, 1998; *Hacker et al.*, 2003], and dehydration reactions eventually take place, accompanied by the release of water to the surroundings.

[27] The subduction of the two oceanic plates under Kanto can generate a more complicated metamorphism than in single-slab subduction environments. The water released from the PAC slab will alter the peridotite in the mantle of the PHS slab, in the mantle of the continental plate, or both, whereas that released from the PHS slab will react with the peridotite in the overlying continental plate. The reaction of water with peridotite produces serpentine minerals with fluid contents of up to ~12 wt%. Serpentine minerals are divided into the three major phases of lizardite, chrysotile, and antigorite: the former two phases are stable at temperatures below 250°C [*Evans*, 1977] and the latter one is stable at higher temperatures of up to 600–700°C [e.g., *Ulmer and Trommsdorff*, 1995; *Schmidt and Poli*, 1998]. The thermal structures calculated by *Iwamori* [2000]

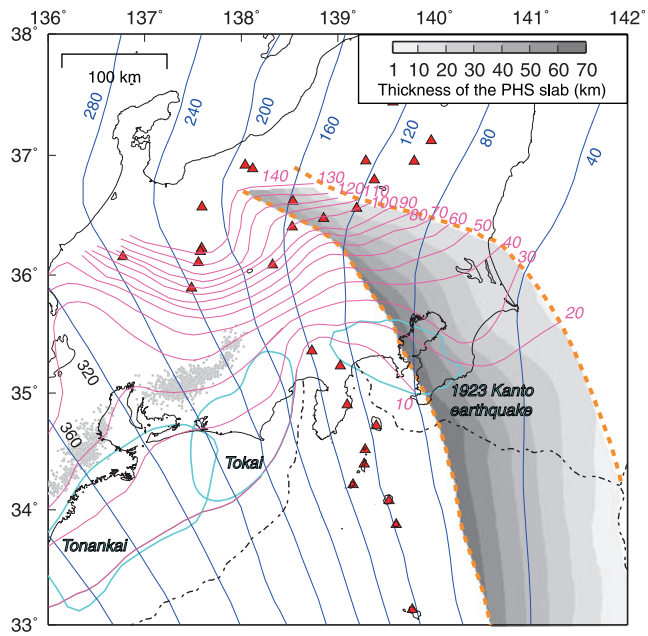

Figure 9. Map showing the isodepth contours of the PAC (blue) and PHS (pink) slabs estimated in this study. An area enclosed by orange dashed lines with gray shading represents the slab contact zone (PHS-PAC interface). The vertical thickness of the PHS slab is shown by gray scales. Light blue areas indicate source areas of megathrust interplate earthquakes [*Wald and Somerville*, 1995; Headquarters for Earthquake Research Promotion, On the long-term evaluation of earthquakes in the Nankai Trough (in Japanese), 2001, available at http://www.jishin.go.jp/main/chousa/01sep_nankai/index.htm]. Red triangles indicate active volcanoes, and gray circles denote nonvolcanic deep tremors [*Obara*, 2002].

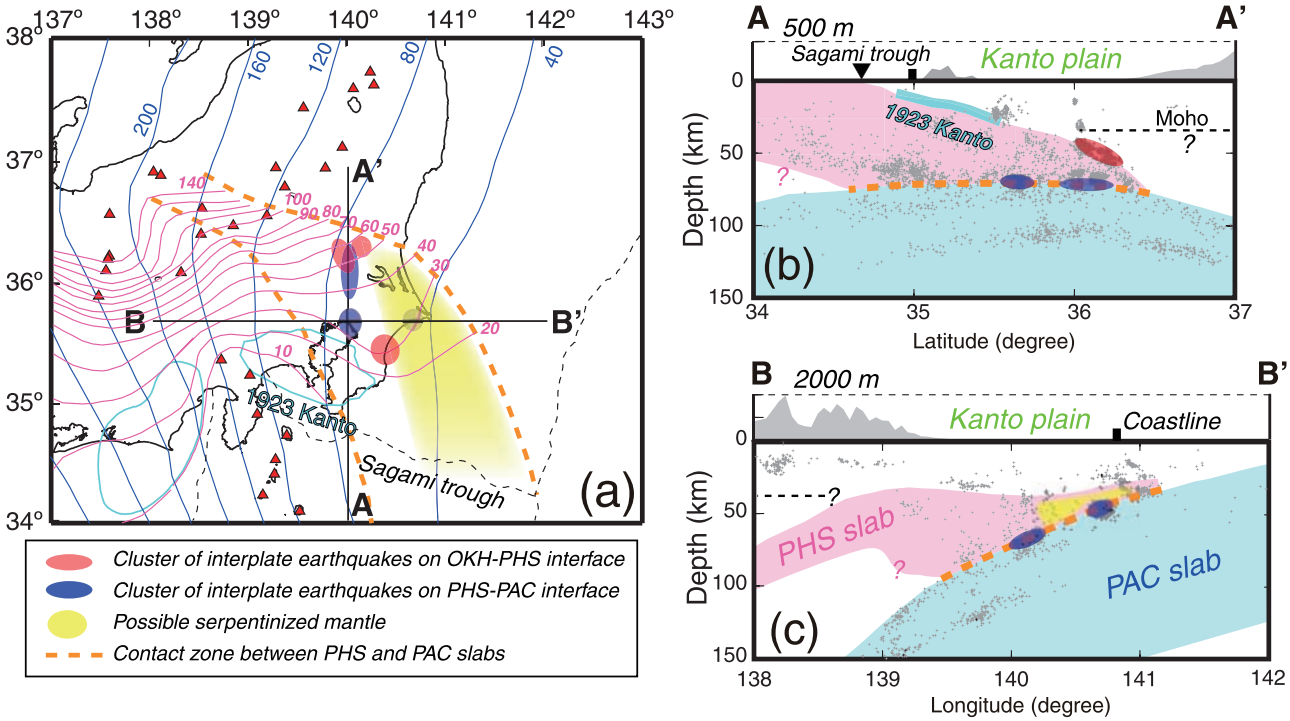

Figure 10. Schematics integrating relevant results obtained in this study. (a) The isodepth contours of the PHS and PAC slabs, the slab contact zone, characteristic interplate seismicity, and the serpentinized mantle of the PHS slab. Vertical cross sections along lines (b) A-A′ and (c) B-B′ in Figure 10a. Gray shadings and black squares at the top of Figures 10b and 10c denote topography and coastline, respectively. The continental Moho is schematically shown by black dashed lines. Source area of the 1923 Kanto earthquake [*Wald and Somerville*, 1995] is shown by a light blue line in Figure 10b.

showed that temperatures beneath Kanto are generally less than 600°C down to a depth of ~50 km, even though his model did not incorporate realistic plate geometry, suggesting antigorite to be stable there. Actually, the existence of serpentinization in the continental mantle wedge has been inferred from geophysical observations such as lower seismic velocities and high Poisson's ratios [e.g., *Kamiya and Kobayashi*, 2000; *Matsubara et al.*, 2005].

[28] Deformation experiments on serpentine have shown that the friction coefficient of chrysotile gouge is as low as 0.2 [*Moore et al.*, 1997] and the viscosity of antigorite is much lower than that of the major mantle-forming minerals [*Hilairet et al.*, 2007]. *Wada et al.* [2008] showed, through numerical simulation, that the presence of hydrous minerals and high fluid pressure weakens the interface between the subducting slab and overlying continental plate. These studies suggest that the presence of serpentine along the slab interface can localize deformation, impede stress build-up, and limit the occurrence of interplate earthquakes.

4. Discussion

[29] We here briefly summarize relevant results obtained in this study. Figure 10 shows schematic illustrations of heterogeneous structures beneath Kanto, as inferred from our observations. The subduction of the PAC and PHS slabs has produced highly complex heterogeneities and has resulted in the overlap of the PHS slab with the PAC slab. The slab contact zone between the two slabs (orange dashed lines) underlies a wider region of the Kanto district. Under this tectonic framework, interplate earthquakes occur along the PHS-PAC interface (purple hatched region) and along the OKH-PHS interface (red hatched region). Furthermore, the easternmost portion of the mantle of the PHS slab underlain by the PAC slab is probably serpentinized (yellow hatched region). Notably, interplate earthquakes do not tend to occur along the PHS-PAC interface overlain by the serpentinized mantle of the PHS slab.

[30] The following sections address these features in detail. First, we describe the overall pattern of the downdip limit of interplate earthquakes on both the PAC and PHS slabs and interpret their deepenings in terms of a lower-temperature environment as a result of the slab-slab contact. Then, we discuss the distribution of interplate earthquakes on each plate interface in relation to the structural heterogeneity above it.

4.1. Anomalously Deep Downdip Limit of Earthquakes Related to the Slab Contact

[31] Figures 11a and 11b show the distribution of interplate earthquakes and small repeating earthquakes [*Uchida et al.*, 2009] along the upper surfaces of the PHS and PAC slabs, respectively. We defined the downdip limit of interplate earthquakes on the PAC slab from the distribution of thrust-type earthquakes as in the work by *Igarashi et al.* [2001]. However, since small interplate earthquakes have rarely occurred on the PHS slab in Tokai, we regarded that the downdip limit of source areas of megathrust earthquakes corresponds to that of interplate earthquakes. The inferred downdip limit of interplate earthquakes along the upper

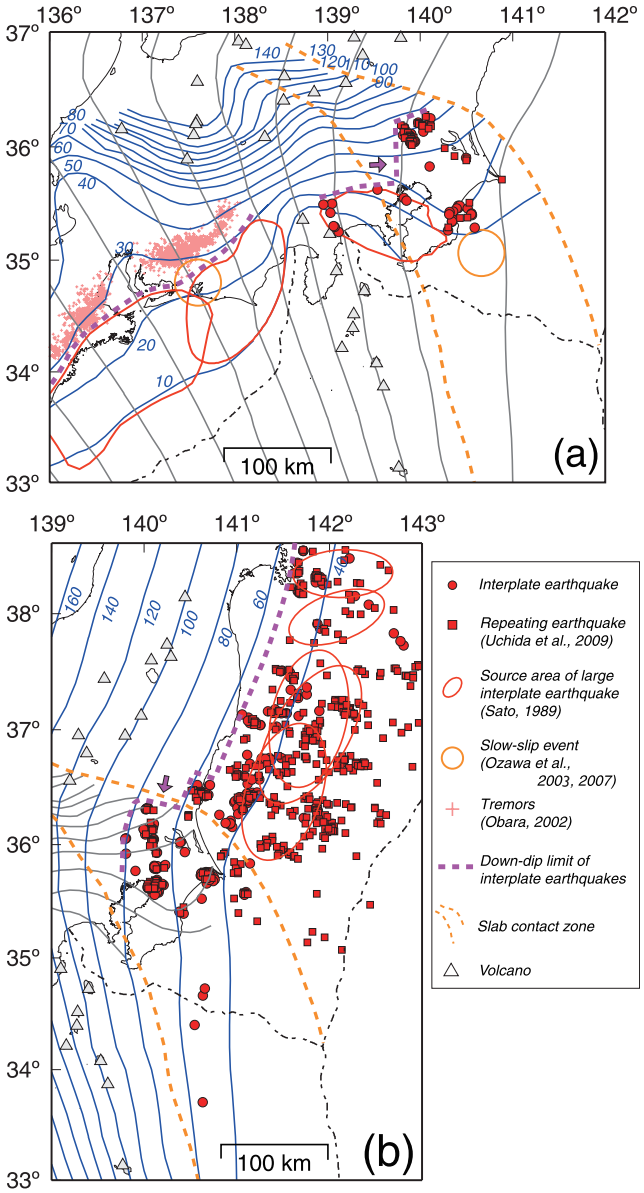

Figure 11. Distribution of interplate earthquakes along the upper surfaces of the (a) PHS and (b) PAC slabs. Location where the downdip limit of interplate earthquakes is deepened is indicated by a purple arrow. Note that all the earthquakes plotted are taken from the JMA unified catalog and are not relocated with the final 3-D velocity model.

surface of the PHS slab deepens abruptly from 20 to 30 km depths to ~60 km above the slab contact zone, and that on the upper surface of the PAC slab also shows a deepening from a depth of ~50 km [e.g., *Igarashi et al.*, 2001] to ~80 km immediately underneath it (purple dashed lines in Figure 11).

[32] *Hyndman et al.* [1997] argued that the downdip limit of interplate earthquakes is controlled either by the temperature (~350°C) at the plate interface or by the Moho of the overlying plate. The former corresponds to frictional property transitions in the crustal materials, from unstable sliding to stable sliding, and the latter is based on the assumption that the mantle wedge is serpentinized, resulting in stable sliding along the plate interface. The deepening of the downdip limits of interplate earthquakes along both slab surfaces in harmony with the lateral extent of the slab contact zone can be, on the whole, associated with temperature conditions, because the downdip limits of interplate earthquakes for the two slabs are much deeper than the depth of the Moho in the overlying continental plate (~30 km).

[33] The abrupt deepening of interplate earthquakes on the PAC slab by ~30 km is probably related to lower-temperature environments as a result of the contact with the overlying PHS slab (Figure 10). The existence of the PHS slab above the PAC slab can hinder effective heat transfer to the upper surface of the PAC slab from the hot mantle wedge. Consequently, temperatures in the PAC slab can retain low enough to cause brittle failure along the plate interface to a depth of ~80 km. The possible lower-temperature conditions of the PAC slab have also been suggested by the distribution of intraslab earthquakes [*Noguchi*, 2007; *Hasegawa et al.*, 2007] and deeper preservation of a low-velocity layer interpreted as hydrated oceanic crust [*Matsubara et al.*, 2005; *Nakajima et al.*, 2009].

[34] We infer that the deepening of interplate earthquakes on the PHS slab beneath Kanto is caused principally by the subduction of the older PHS slab (>48 Ma) [*Seno and Maruyama*, 1984] compared to that beneath Tokai, where a younger slab (15–27 Ma) [*Okino et al.*, 1994] is subducting. However, the downdip limit of interplate earthquakes on the PHS slab beneath Kanto (~60 km) is comparable to or slightly deeper than that on the PAC slab beneath NE Japan (~50 km) [*Igarashi et al.*, 2001] at the age of ~130 Ma. Therefore, the cooling effect by the much colder PAC slab subducting below would also contribute to the deepening of interplate earthquakes on the PHS slab, even though precise estimation of the thermal structure using a realistic tectonic framework is required for quantitative evaluation.

4.2. Thrust-Type Earthquakes on the PHS Slab

4.2.1. Does Serpentinized Mantle Wedge Exist in the Overlying Continental Plate?

[35] A prominent E–W trending low-velocity anomaly at depths of 25–50 km (R-R′ in Figure 12) has been pointed out by previous studies [e.g., *Ohmi and Hurukawa*, 1996; *Kamiya and Kobayashi*, 2000, 2007; *Sekiguchi*, 2001; *Seno et al.*, 2001; *Matsubara et al.*, 2005; *Wu et al.*, 2007]. The low-velocity zone partly shows a high-attenuation anomaly [*Nakamura et al.*, 2006] and is interpreted as serpentinized mantle wedge in the overlying continental plate [*Kamiya and Kobayashi*, 2000; *Matsubara et al.*, 2005, 2008], low-density crust of the PHS slab [*Ohmi and Hurukawa*, 1996; *Sekiguchi*, 2001], or lower crustal materials in the overlying plate carried downward by tectonic erosion [*Wu et al.*, 2007].

[36] The low-velocity zone can be classified into two parts at a depth of 30 km (Figure 12a). The low-velocity zone north of the 30 km isodepth contour of the PHS slab is located in the overlying continental plate, whereas that south of it corresponds to the crust of the PHS slab. Since seismic velocities of this low-velocity zone located in the overlying plate are 6.5–7.0 km/s for P waves, 3.6–4.0 km/s for S waves, and ~1.8 for Vp/Vs, the low-velocity anomaly can be explained either by serpentinized peridotite [e.g.,

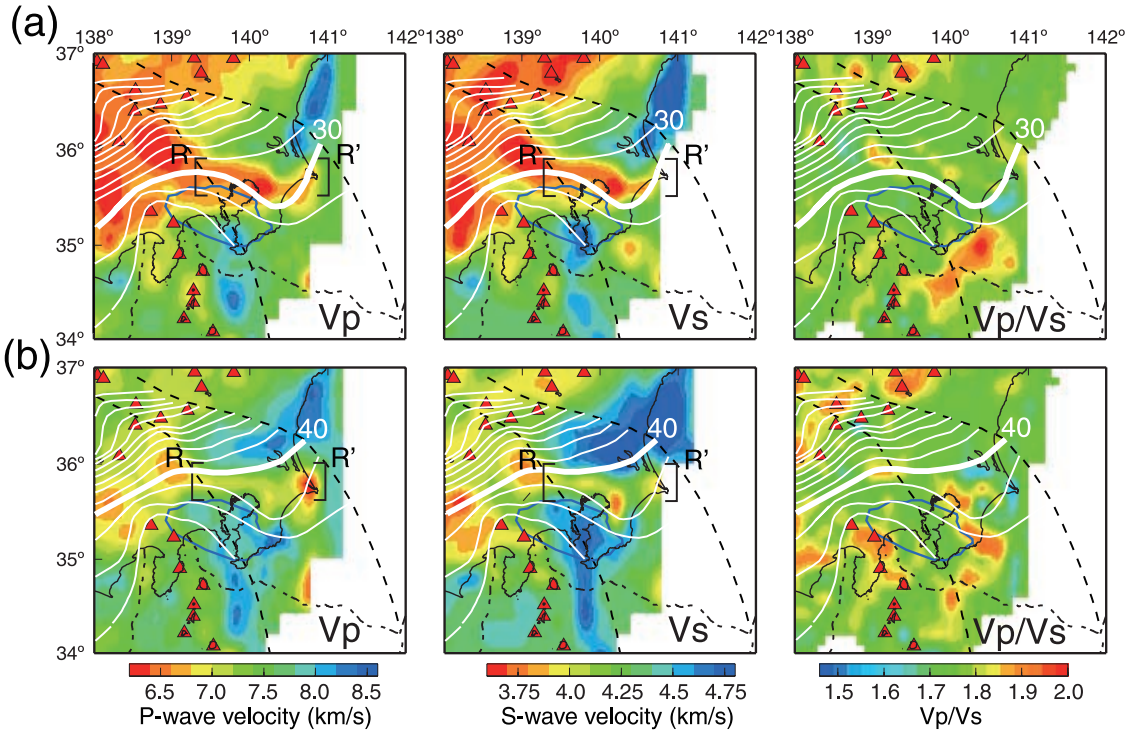

Figure 12. Map showing P and S wave velocities and Vp/Vs ratios at depths of (a) 30 km and (b) 40 km, together with the isodepth contours of the PHS slab with an interval of 10 km. The area labeled R-R′ shows the E–W trending low-velocity zone discussed in the text. The slab contact zone is shown by black dashed lines, and volcanoes are indicated by red triangles. Source area of the 1923 Kanto earthquake [*Wald and Somerville*, 1995] is enclosed by light blue line.

Hacker et al., 2003] or lower crustal materials [e.g., *Nishimoto et al.*, 2008]. Therefore, whether or not serpentinized mantle exits at that depth depends on the configuration of the continental Moho. The precise geometry of the Moho is essential to determine the cause of the E–W trending low-velocity anomaly at a depth of ~30 km.

[37] At a depth of 40 km, the low-velocity anomaly running in the E–W direction corresponds evidently to the crust of the PHS slab, since the 40 km isodepth contour of the PHS slab is located just north of it (Figure 12b). This suggests the absence of a low-velocity anomaly in the overlying continental plate beyond a depth of 40 km. This interpretation is robust even if we refer to the 40 km isodepth contour of the PHS slab estimated by *Hori* [2006]. We thus conclude that the mantle wedge in the overlying plate does not show the low-velocity anomaly beyond a depth of 40 km, which in turn suggests that serpentinized mantle wedge could be possible in a narrow depth range between the continental Moho and a depth of 40 km.

4.2.2. Distribution of Interplate Earthquakes

[38] Figures 13a–13c show P and S wave velocity and Vp/Vs ratio distributions at 5 km above the upper surface of the PHS slab, together with the distribution of interplate earthquakes along the OKH-PHS interface. Figures 13a–13c can characterize the correlation between the distribution of interplate earthquakes on the OKH-PHS intrface and the heterogeneity in the lowermost part of the continental plate. Interplate earthquakes along the OKH-PHS interface mainly occur in two regions: in shallower regions around the source area of the 1923 Kanto earthquake at depths of 10–30 km and in deeper regions at depths of 40–60 km. A seismicity gap of interplate earthquakes exists between the two regions (white shaded region labeled with S in Figure 13a).

[39] Several clusters of shallower interplate earthquakes are distributed around the source area of the 1923 Kanto earthquake, where seismic coupling is considered to be strong in interseismic periods. One of the predominant clusters exists to the northeast of the source area (V in Figure 13c), where the PHS slab is probably in contact with the lower crust of the overlying continental plate. Around this cluster, slow slip events with ruptures propagating southward have occurred along the OKH-PHS interface with an interval of ~5 years [e.g., *Ozawa et al.*, 2003, 2007]. Interplate earthquakes on the interface slab are usually accompanied by slow slip events [*National Institute for Earth Science and Disaster Prevention*, 2007]. Since seismic velocities in the overlying continental plate immediately above the cluster V show slightly higher values than the surroundings (Figures 13a and 13b), small patches (asperities) along the OKH-PHS interface can slip seismically and cause concentrated interplate earthquake activity.

[40] The deeper interplate earthquakes (U in Figure 13c) consist of two concentrated clusters. Remarkably, the seismic velocities in the continental plate above these clusters are, on the whole, faster than 8.0 km/s for P waves and 4.5 km/s for S waves, which correspond to those of peridotite without metamorphism [e.g., *Christensen*, 1996; *Hacker et al.*, 2003]. These results suggest that serpentinization in the overlying continental plate does not control the

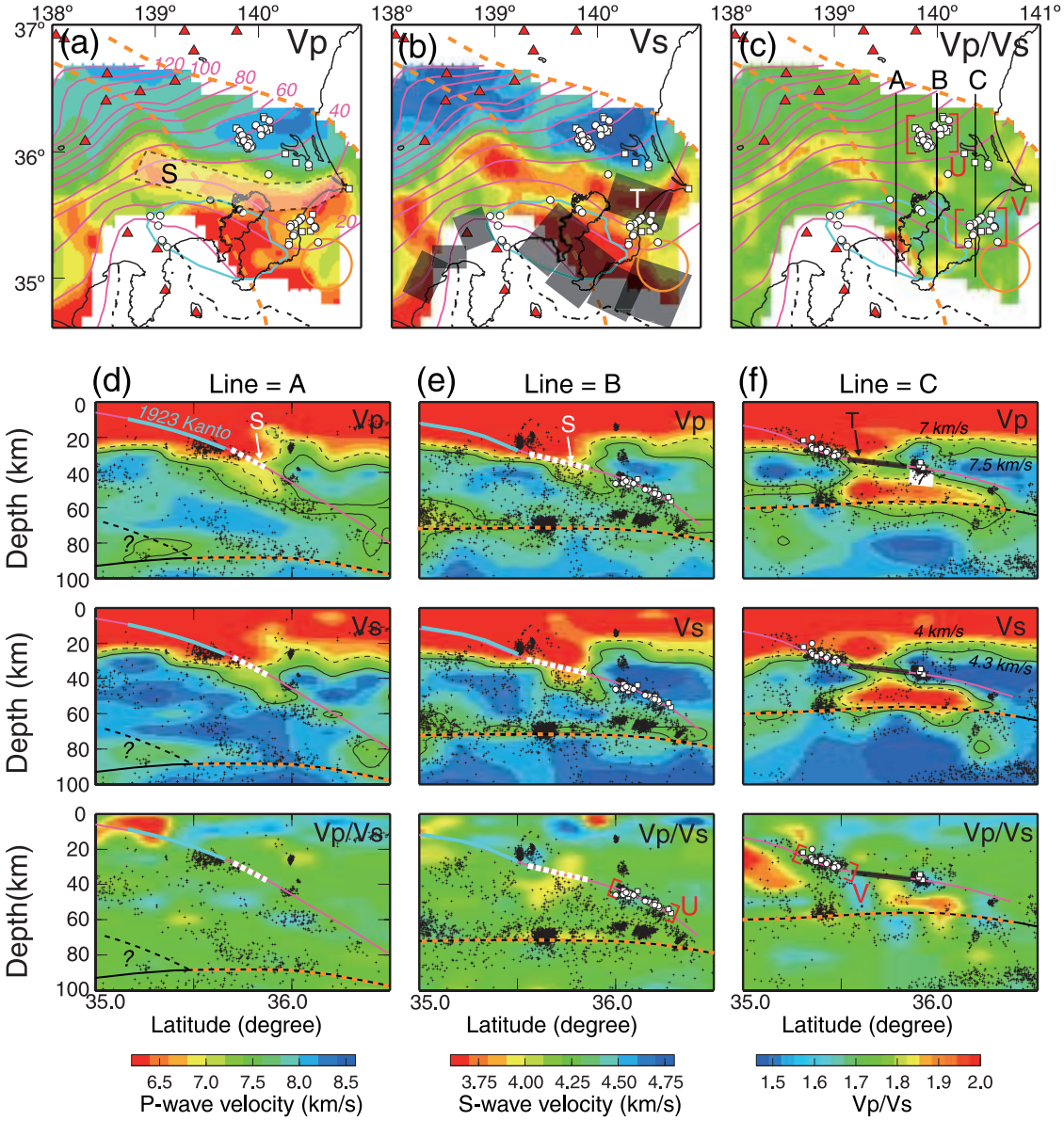

Figure 13. Seismicity along the upper surface of the PHS slab. Distributions of (a) P wave velocities, (b) S wave velocities, and (c) Vp/Vs ratios along the curved surface 5 km above the PHS slab. North-south vertical cross sections of P and S wave velocities and Vp/Vs ratios along lines (d) A, (e) B, and (f) C shown in Figure 13c. White circles and squares denote interplate earthquakes and small repeating earthquakes [*Uchida et al.*, 2009] along the upper surface of the PHS slab (OKH-PHS interface), respectively. Other earthquakes are shown by crosses in Figures 13d–13f. All the plotted earthquakes are relocated with the 3-D velocity model. The high seismic coupling areas (>70%) along the OKH-PHS interface estimated by geodetic data [*Nishimura et al.*, 2007] are shown by gray rectangles in Figure 13b. The seismic gap labeled as S in Figure 13a, high seismic coupling area labeled as T in Figure 13b, and two seismicities labeled as U and V in Figure 13c are discussed in the text. Light blue area and orange circles in Figures 13a–13c denote source areas of the 1923 Kanto earthquake [*Wald and Somerville*, 1995] and slow slip events [*Ozawa et al.*, 2003, 2007], respectively. Pink and black lines in Figures 13d–13f represent the upper surface of the PHS and PAC slabs estimated in this study, respectively, and orange dashed lines in Figures 13d–13f represent the slab contact zone (PHS-PAC interface). The approximate location of the bottom of the PHS slab is shown by a black dashed line in Figure 13d. Light blue lines along the OKH-PHS interface in Figures 13d and 13e denote the source area of the 1923 Kanto earthquake [*Wald and Somerville*, 1995]. Isovelocity contours of 7.0 and 7.5 km/s for P waves and 4.0 and 4.3 km/s for S waves are shown in corresponding cross sections. White dashed lines in Figures 13d and 13e and gray lines in Figure 13f along the OKH-PHS interface represent the seismic gap and high seismic coupling area, respectively.

occurrence of interplate earthquakes, and hence other candidates must be responsible for much of the localization of the seismic patches (asperities) along the OKH-PHS interface. We acknowledge that subducting seamounts on the subducting PHS slab or finer-scale heterogeneity in the continental plate, which are not resolved in this study, may exist and generate distinct clusters of interplate earthquakes in small areas, even though there is no seismological evidence for such candidates.

4.2.3. Seismic Gap of Interplate Earthquakes on the PHS Slab at Depths of 30–40 km

[41] We here discuss the absence of interplate earthquakes at depths of 30–40 km between the shallower and deeper clusters (white shaded region S in Figure 13a), in terms of the possibility of the occurrence of future large interplate earthquakes. *Kamiya and Kobayashi* [2000] suggested that the presence of serpentinized mantle in region S controls the downdip limit of the 1923 Kanto earthquake. *Seno* [2005, 2007] also interpreted that the absence of interplate earthquakes in that region is due to serpentinization in the overlying continental plate and pointed out a low probability of earthquakes to be generated there. However, combined analysis of recent GPS data with leveling data by *Nishimura et al.* [2007] revealed an isolated seismic coupling region (>70%) along the OKH-PHS interface (gray shaded region T in Figure 13b), with implications for the occurrence of large interplate earthquakes there.

[42] Our results show that a seismic gap of interplate earthquakes along the OKH-PHS interface (white broken lines in Figures 13d and 13e) is sandwiched by the low-velocity materials of the continental plate and the PHS slab. The low-velocity materials below the OKH-PHS interface correspond to the hydrated oceanic crust [*Matsubara et al.*, 2005; *Hirose et al.*, 2008a]. Even if the low-velocity materials in the continental plate reflect serpentinized mantle, lower crustal materials, or both, the low-velocity materials above the OKH-PHS interface may promote ductile (aseismic) deformation along it. If this is the case, it would be unlikely for large thrust earthquakes to take place there, which is inconsistent with the plate coupling estimated by *Nishimura et al.* [2007]. Reevaluation of the seismic coupling region using the updated model of the PHS slab as well as an investigation of the physical (frictional) properties of the low-velocity anomaly around the OKH-PHS interface is of considerable importance for a more realistic evaluation of the seismic hazard for the Tokyo metropolitan area.

4.3. Interplate Earthquakes Along the PHS-PAC Interface: Spatial Correlation to Metamorphism at the Lowermost Part of the PHS Slab

[43] In order to characterize the spatial relationship between the occurrence of interplate earthquakes on the PHS-PAC interface and the structural heterogeneity above it, we calculated P and S wave velocity and Vp/Vs distributions along the curved surface 5 km above the PAC slab (Figures 14a–14c). An area with a prominent low-velocity and partly high Vp/Vs ratio (1.8–1.9) is observed in the eastern half of the slab contact zone. The low-velocity zone has a maximum thickness of ~30 km and appears to extend from the Sagami trough to the northern limit of the PHS slab. The zone with P and S wave velocities of 6.5–7.5 km/s and 3.75–4.25 km/s, respectively, can be explained either by crustal materials in the PHS slab or by metamorphosed peridotite in the PHS slab [e.g., *Hacker et al.*, 2003]. The uppermost part of the low-velocity anomaly is probably attributable to the hydrated crust of the PHS slab.

[44] By a seismic refraction survey, *Kamimura et al.* [2002] detected serpentinized materials in the PHS plate above the PAC plate at the Izu-Bonin subduction zone, where a chain of serpentine seamounts is exposed at the fore-arc slope 40–50 km west of the Izu-Bonin trench axis. The lateral extent of the serpentinized materials is ~100 km and P wave velocities range from 6.4 km/s to 7.3 km/s, which are comparable to those of the low-velocity anomaly observed in this study. We thus infer that serpentinized mantle, which had formed in the PHS plate before subduction and has been retained even after the subduction because of the extremely low-temperature environment resulting from the slab-slab contact, is responsible for the low-velocity anomaly observed in the mantle of the PHS slab. Even though metamorphism in the PHS slab could have occurred after the subduction by reaction with fluids supplied from the PAC slab subducting below, the contribution may be small because large-scale serpentinization is not observed at the same depths in the mantle wedge of northeastern Japan, where the PAC slab is also subducting.

[45] We noticed a spatial correlation between the serpentinization in the PHS slab and the occurrence of interplate earthquakes along the PHS-PAC interface. For example, an N–S trending cluster of interplate earthquakes (W in Figure 14) is located immediately west of the downdip limit of the serpentinized mantle. Cluster X also appears to be distributed in an area where seismic velocities at the lowermost part of the PHS slab are not extremely low, although traveltime tomography with higher spatial resolution is required for further confirmation. In contrast, interplate earthquakes are almost absent along the PHS-PAC interface, above which high-degree serpentinization is expected in the PHS slab (an area labeled Y). These observations can be explained as follows. The PHS-PAC interface overlain by unmetamorphosed mantle can cause seismic slips of small asperities (patches) surrounded by stable sliding, whereas that overlain by serpentinized mantle can promote stable sliding because of its much low viscosity, resulting in the absence of interplate earthquakes there [e.g., *Moore et al.*, 1997; *Hilairet et al.*, 2007].

5. Conclusions

[46] This paper estimated the detailed 3-D seismic velocity structures around the Kanto district and the precise configurations of the upper surfaces of the PAC and PHS slabs. We discussed seismotectonics beneath Kanto in terms of slab-slab contact, the resultant lower-temperature environment for the two slabs, and the metamorphism of the PHS slab. The main conclusions are as follows:

[47] 1. We updated the configuration of the upper surface of the PAC slab beneath Kanto on the basis of the distributions of interplate and intraslab earthquakes relocated by a 1-D velocity model with station corrections and elevation of stations.

[48] 2. We delineated the upper surface of the PHS slab beneath Kanto and Tokai from the 3-D seismic velocity

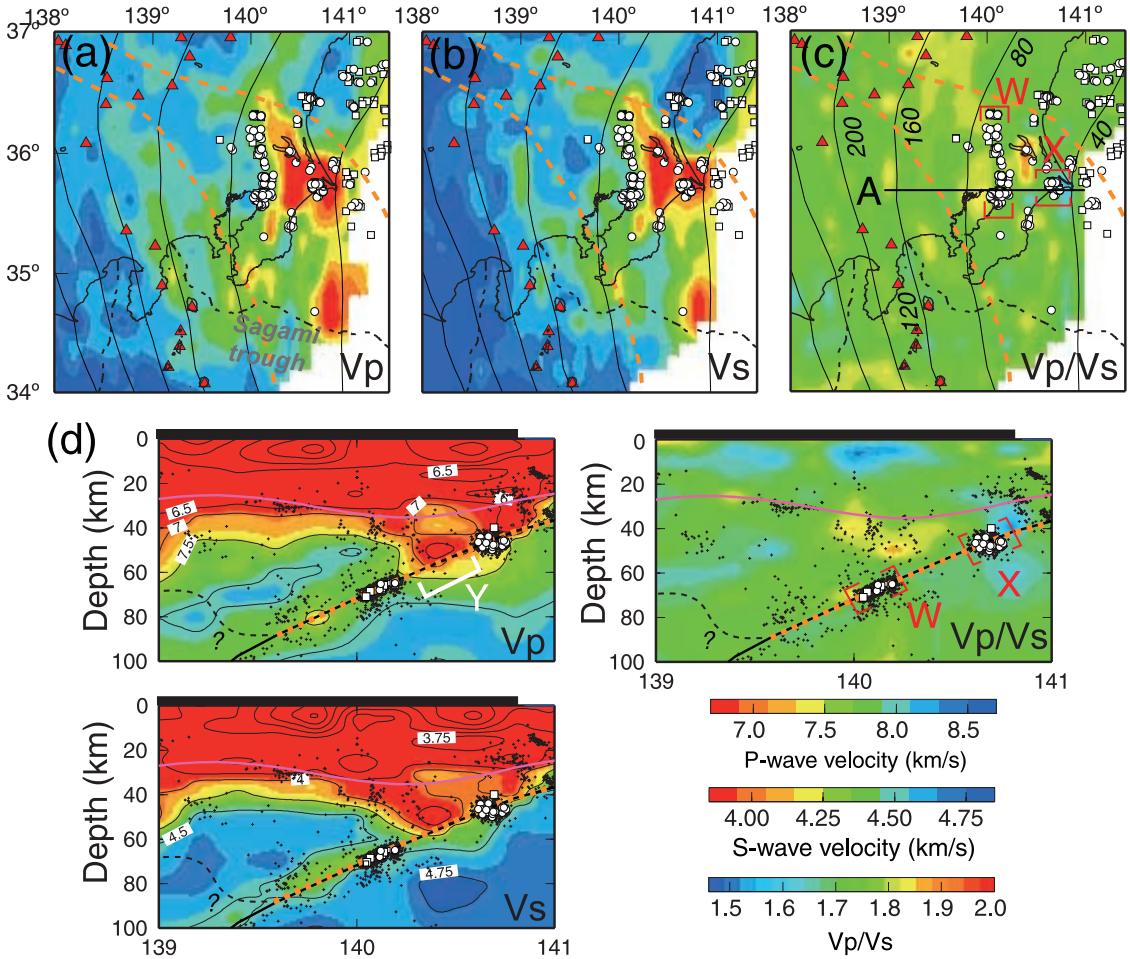

Figure 14. Seismicity along the upper surface of the PAC slab. Distributions of (a) P wave velocities, (b) S wave velocities, and (c) Vp/Vs ratios along the curved surface 5 km above the PAC slab. (d) East-west vertical cross sections of P and S wave velocities and Vp/Vs ratios along line A in Figure 14c. Isodepth contours of the PAC slab are shown by black lines with an interval of 40 km. White circles and squares denote interplate earthquakes and small repeating earthquakes, respectively, along the upper surface of the PAC slab. The seismicities labeled W and X in Figure 14c and the seismic gap of interplate earthquakes on the Pacific slab shown by Y in Figure 14d are discussed in the text. The other symbols are the same as in Figure 13.

structures obtained by traveltime tomography, and revealed that the PHS slab is subducting toward the northwest of the Izu collision zone without a gap (slab window) between Kanto and Tokai. In that area, the PHS slab can be detected down to depths of 130–140 km.

[49] 3. On the basis of the configurations of the PHS and PAC slabs, we defined the lateral extent of the contact zone between the two slabs. The lateral extent of this slab contact zone underlies a wider area of Kanto and corresponds well to that of the Kanto plain.

[50] 4. The downdip limits of interplate earthquakes on the PHS and PAC slabs abruptly become deeper by ~30 km only above and underneath the slab contact zone, respectively. These deepenings can be due to lower-temperature conditions resulting from the overlapping of the two slabs.

[51] 5. An east-west trending prominent low-velocity zone imaged at a depth of 40 km beneath Kanto corresponds to the crust of the subducting PHS slab, which is suggestive of the absence of large-scale serpentinized mantle wedge in the continental plate beyond a depth of 40 km.

[52] 6. A prominent low-velocity zone was detected in the PHS slab in the eastern half of the slab contact zone, which is probably caused by the serpentinized mantle of the PHS slab. The spatial correlation that interplate earthquakes are almost absent along the PHS-PAC interface underlain by serpentinized mantle can be explained by the promotion of aseismic creep because of the ductility of serpentine.

[53] This study qualitatively demonstrated the importance of the slab-slab contact and overlap on seismotectonics beneath Kanto. Further quantitative analyses of the effects of the contact zone on the thermal structures in and around both slabs, as well as the mechanical interactions between the two slabs, will enhance our understanding of the unique and complex tectonics in this region and provide further constraints for realistic seismic hazard evaluation of

the highly populated Tokyo metropolitan area and its surroundings.

Appendix A: JMA Unified Catalog and 1-D Velocity Inversions

A1. Unified Hypocenter Catalog by the Japan Meteorological Agency

[54] Seismograph stations throughout the Japanese Islands have been installed and maintained by universities, the National Research Institute for Earth Science and Disaster Prevention (NIED), the Japan Meteorological Agency (JMA), national institutes, and local governments. Since October 1997, short-period seismograms recorded at these stations have been transmitted to the JMA. The JMA has processed the data to produce a comprehensive seismic catalog for Japan (so-called, unified JMA catalog). Data from Hi-net stations, a dense network of highly sensitive short-period instruments installed by the NIED, have been included in the database since October 2000 [*Okada et al.*, 2004] and have remarkably improved the detection ability. One of the advantages of the JMA catalog is that it provides almost the same detectability beneath all of the Japanese Islands, due to a densely deployed nationwide seismograph network composed of more than 1200 stations with a station separation of ~20 km. Hypocenters in the JMA unified catalog are determined using the 1-D velocity model (JMA2001) of *Ueno et al.* [2002] (black curves in Figure A1).

[55] The hypocenters in the JMA unified catalog have, however, two disadvantages. One is the neglect of station elevations during the calculation of hypocenters, and the other is a lack of consideration of station corrections for OBS stations [*Harada*, 2004]. These disadvantages will be minor in most cases because station elevations are usually less than 1000 m and OBS stations are deployed only in some limited areas. However, they would have critical effects when trying to estimate the precise hypocenter distributions and detailed seismic velocity structures beneath Kanto, as in the present study. The Kanto district is covered with thick sediments of up to 4000 m, and hence most of the stations installed by NIED (Hi-net stations) are borehole types with depths of 1000–4000 m [*Okada et al.*, 2004] (Figure A2b). In addition, 13 OBS stations have been deployed off Kanto from 600 to 4000 m below sea level by the NIED, JMA, and Earthquake Research Institute, University of Tokyo (Figure A2b). The station corrections for the OBS stations installed by NIED were estimated to be up to 1.5 s [*Matsubara et al.*, 2005]. The arrival times of earthquakes that occurred off the Boso and Izu peninsulas are usually picked by these OBS stations, and the ratio of OBS stations relative to all the stations at which P and S wave arrival times were read reaches 40% for some earthquakes. Therefore, the hypocenters in and around the Kanto district need to be relocated using an appropriate velocity model that considers station elevations and station corrections.

A2. One-Dimensional Inversion and Hypocenter Relocation

[56] In order to estimate an appropriate 1-D velocity model and station corrections, we simultaneously inverted the P and S wave arrival times using the inversion program VELEST [*Kissling et al.*, 1994]. Earthquakes for the VELEST inversions were selected based on the following criteria. First, earthquakes (M > 3) that satisfy the following condition were selected: $H^{dep} > D^{min}$, where H^{dep} is a depth of earthquake and D^{min} is an epicentral distance to the nearest station with pickings of P or S wave arrival times. This criterion keeps earthquakes whose depth can be well constrained. Then, we selected one earthquake with the largest number of arrival time data in each block by dividing the study area into 0.1° × 0.1° × 10 km blocks, which yields the distribution of earthquakes in the study area as uniform as possible. In this manner, 658 earthquakes were selected (Figure A2a). We adopted a stratified JMA2001 velocity model [*Ueno et al.*, 2002] as the initial P and S wave velocity models for the VELSET inversions (blue broken lines in Figure A1), and the thickness of the layers was set to be 3–10 km at depths of 0–40 km and 20–50 km at deeper depths.

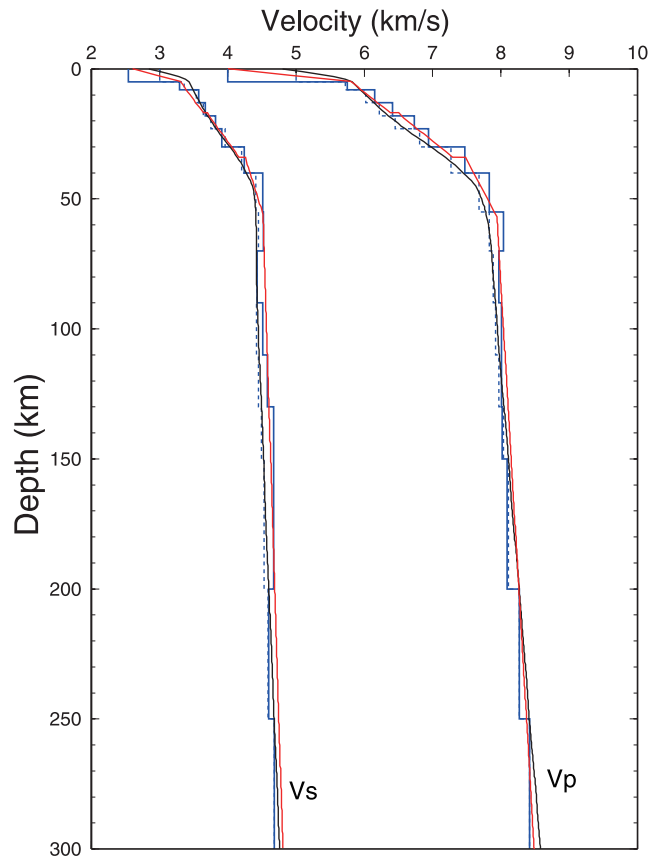

Figure A1. One-dimensional P and S wave velocities for four models. Black curve denotes the velocity model by the JMA2001 [*Ueno et al.*, 2002]. Blue dashed and blue solid lines represent an input velocity model for the VELEST inversions and the final velocity model by the VELEST inversions, respectively. Red curve represents an input velocity model for seismic tomography.

[57] The final 1-D velocity model obtained by the VELEST inversions is shown by blue solid lines in Figure A1. The P and S wave velocities in the uppermost layer became to be much lower than the JMA2001 model, which can reflect a thick sedimentary layer below the Kanto plain, and those in

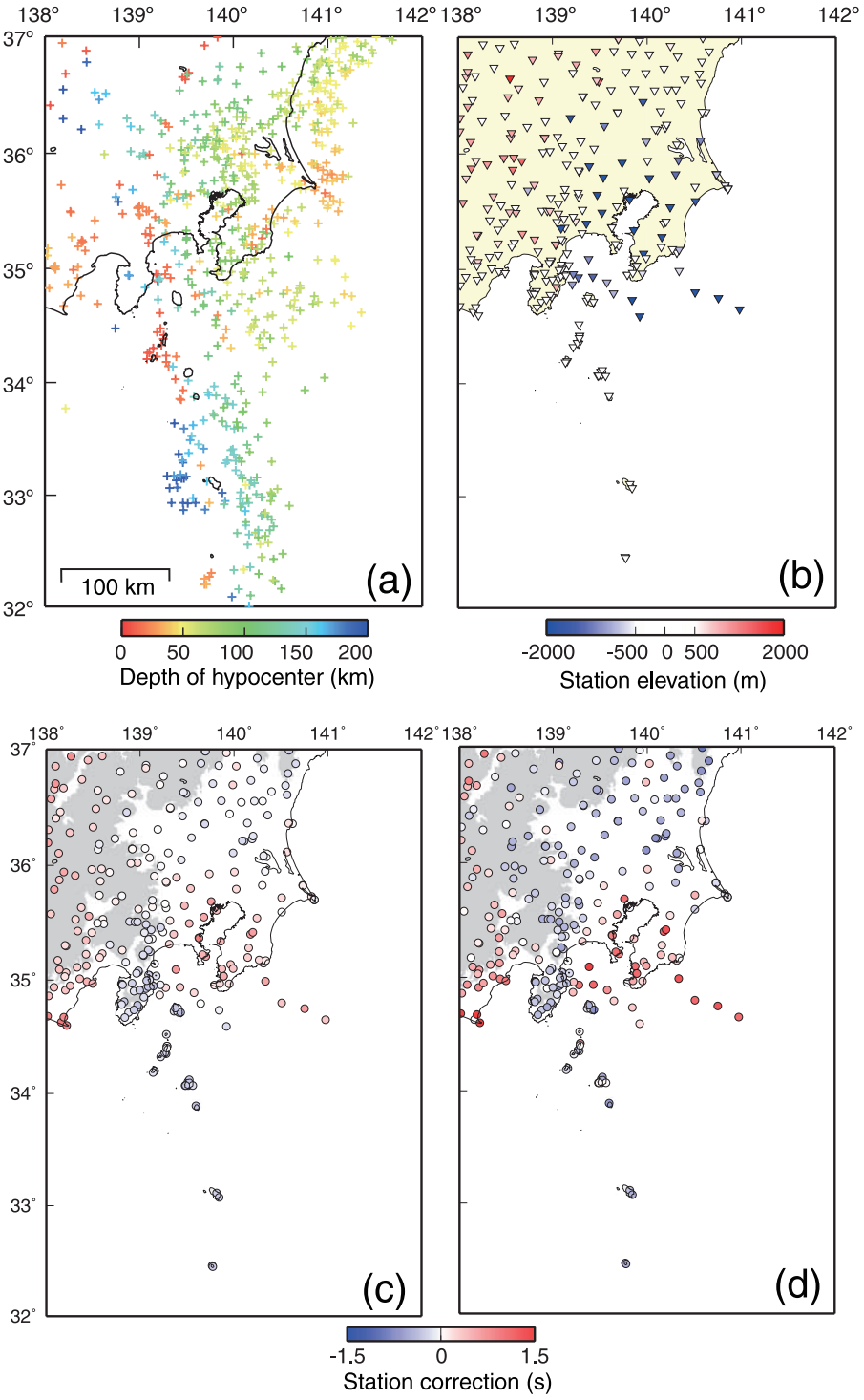

Figure A2. (a) Distribution of the 658 earthquakes used in the VELEST inversions. Colors represent the depths of hypocenters. (b) Distribution of seismograph stations used in VELEST inversions. Colors represent the station elevations relative to the sea level. (c) Station corrections for P waves. (d) Station corrections for S waves. Gray areas in Figures A2c and A2d denote the areas with elevations of >500 m.

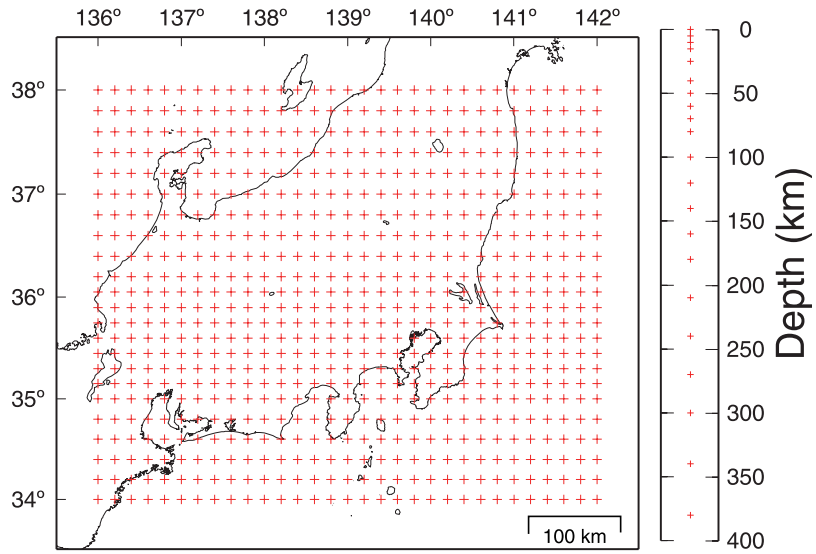

Figure B1. Configuration of the grid nodes adopted in the inversion. Grid spacing in the horizontal direction is 0.15–0.2°. Grid nodes are set up at depths of 0, 10, 15, 25, 40, 50, 60, 70, 80, 100, 120, 140, 160, 180, 210, 240, 270, 300, 340, and 380 km.

the crust became faster than the JMA2001 model. Station corrections for the P and S waves showed clear regional variations (Figures A2c and A2d): the station corrections for stations in mountain ranges were generally negative and those for stations in the plains were mostly positive. The regional pattern of station corrections are similar to those obtained by *Matsubara et al.* [2005] and *Kimura et al.* [2006]. Station corrections for stations located in the southern part of Kanto, where thick sediments are accumulated, were estimated to be up to ~1.0 s for P waves and ~1.5 s for S waves (Figures A2c and A2d). The station corrections for OBS stations were generally positive and reached up to ~2 s.

Appendix B: Traveltime Tomography

B1. Data and Method

[58] We used the arrival time data of 4739 earthquakes (M > 2.0) with focal depths <150 km and 601 ones with focal depths >150 km that occurred in the period from January 2001 to December 2007. P and S wave arrival times of these earthquakes were picked manually in our Institute of Tohoku University, which produced 707,403 P and 427,483 S wave arrival times. In order to improve the resolution at depths greater than 100 km, we added 1168 earthquakes with focal depths greater than 150 km from 1997 to 2007, which were not included in the above data set. Arrival time data for these earthquakes were taken from the JMA catalog (28,117 for P waves and 16,566 for S waves).

[59] We applied tomographic method of *Zhao et al.* [1992a] to a large number of P and S wave arrival time data to determine 3-D P and S wave velocity structures. Perturbations to hypocentral parameters and velocities were determined simultaneously in each iteration. The iterations were terminated when the reduction of the root mean square (RMS) of the arrival time residuals became less than 0.01 s. The damping parameters assigned in the inversion (100 for P waves and 500 for S waves) were selected from a trade-off curve between the data and model variances. Further details of the method are given by *Zhao et al.* [1992a]. Station elevations were precisely evaluated in the 3-D inversions, but station corrections were not considered since they can be expressed as velocity heterogeneities at the near surface.

[60] The model space covered latitudes in the range of 34°–38°N, longitudes in the range of 136°–142°E, and depths in the range of 0–400 km. We set grid nodes with spacing of 0.15–0.2° in the latitude, 0.2° in the longitude directions, and 5–20 km in the vertical direction for depths of <180 km and 30–40 km for greater depths (Figure B1). Denser grid nodes with 0.15° spacing were set up in a latitude range of 35–36.2°N to obtain smaller-scale heterogeneous structures. Although the data set used in this study can resolve smaller-scale structures at depths of <~100 km by the grace of a lot of crossing rays, one of the main targets in this study is to resolve heterogeneous structures related to the Philippine Sea slab at depths of 80–150 km.

B2. Resolution Tests and Uncertainties in Velocity Model

[61] We carried out checkerboard resolution tests (CRTs) to ascertain the adequacy of ray coverage and the reliability of the obtained images. In the CRTs, positive and negative velocity perturbations of 6% were alternately assigned to the grid nodes along both the horizontal and vertical directions, and the travel times for this model were calculated to generate synthetic data. Synthetic data were constructed from the same source-receiver geometry as the observations, with random noises corresponding to phase-picking errors (a standard deviation of 0.1 s for P waves and 0.2 s for S waves). Then, we inverted the calculated synthetic traveltime data using an initial model without any velocity anomalies. Figure B2 shows a good resolution in the whole

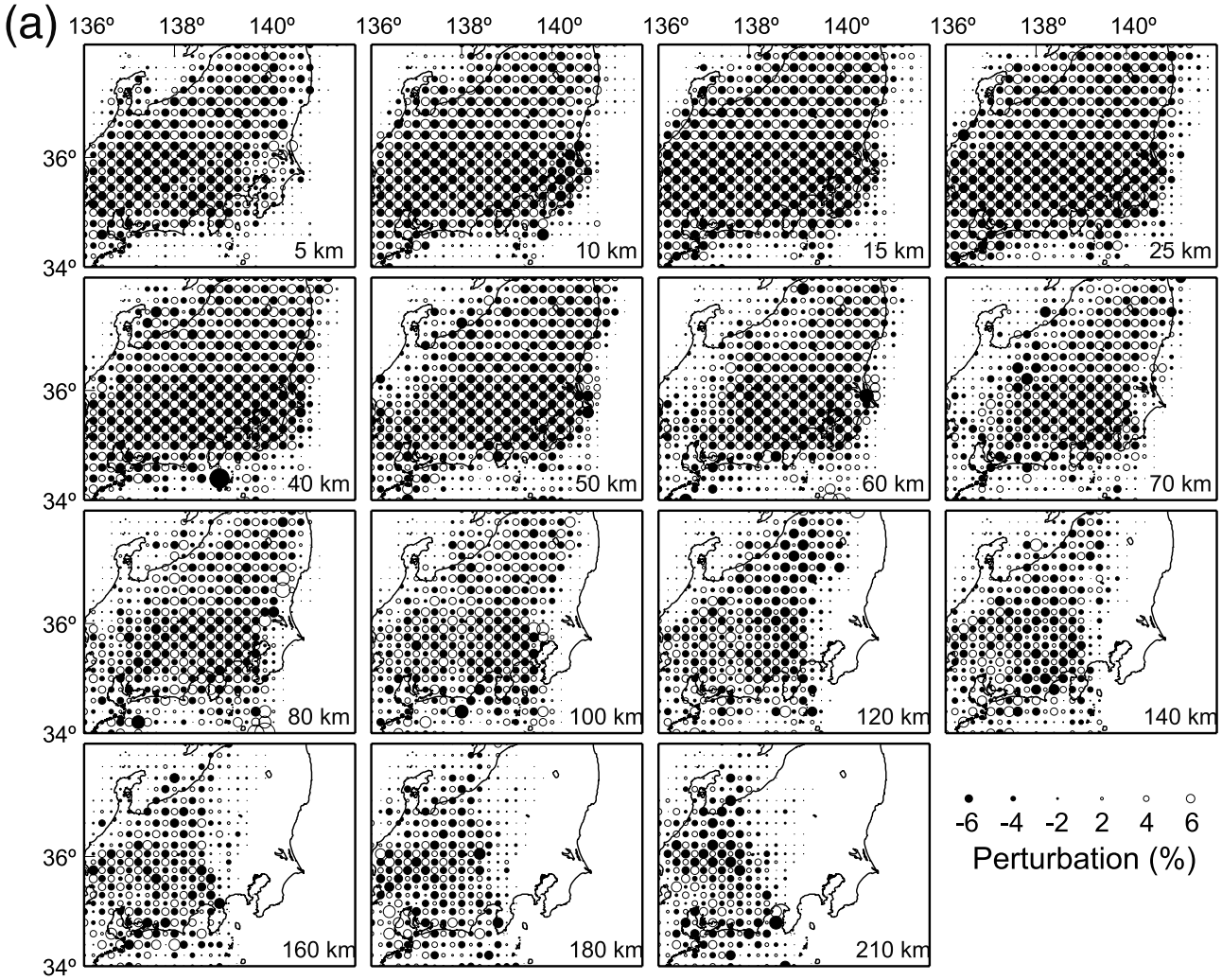

Figure B2. Results of the checkerboard resolution tests for (a) P and (b) S waves. Solid and open circles denote low and high velocities, respectively. The depth of the layer is shown at the bottom right corner of each panel.

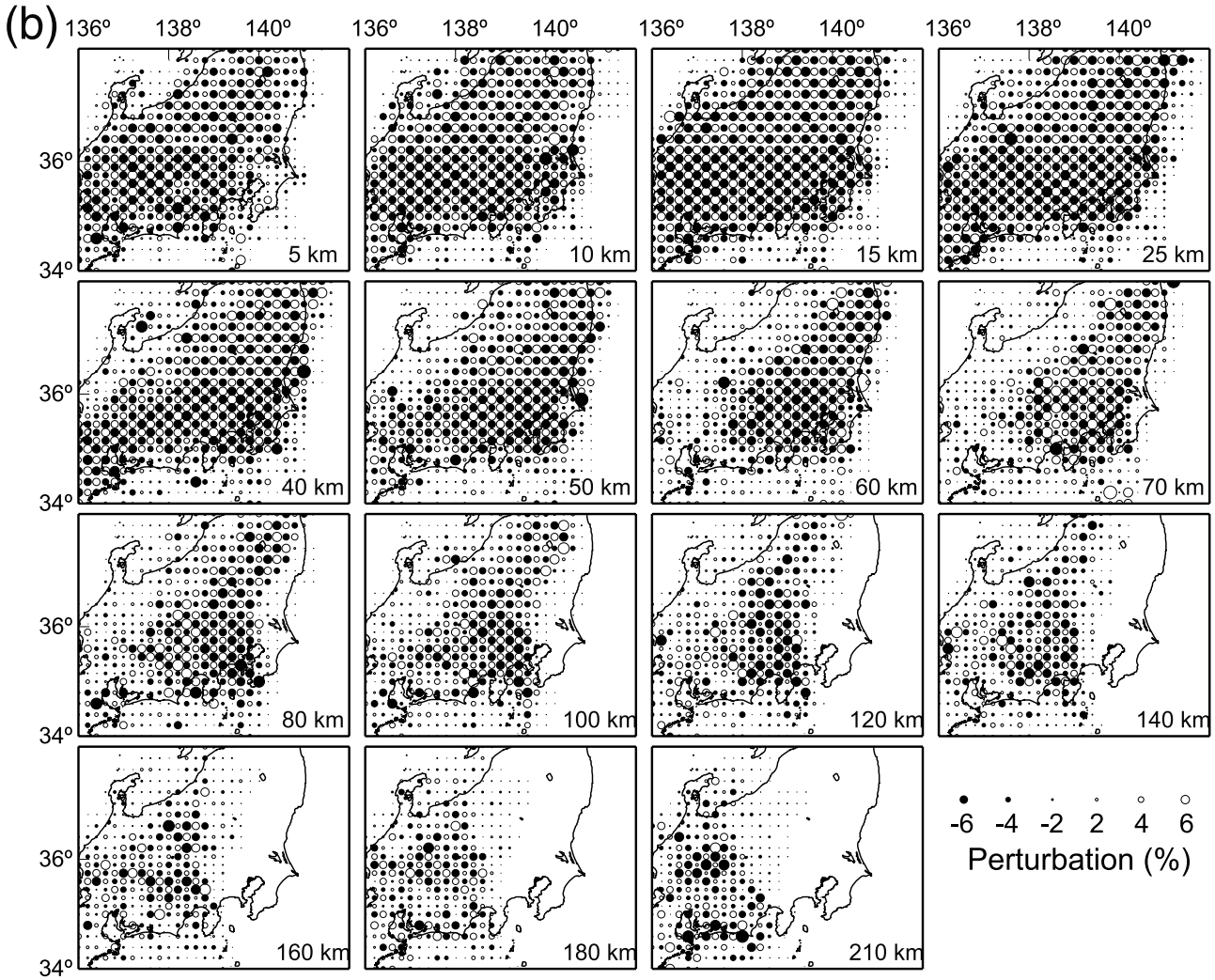

Figure B2. (continued)

study area down to a depth of 50 km. At deeper depths, the checkerboard patterns are not well reconstructed in the western part of the study area (west of ~138°E) where the crossing rays may not be sufficient to resolve the heterogeneous structures comparable to one grid node. However, the northwest area of the Izu collision zone (latitude of ~36°N and longitude of ~139°E) shows good resolution for both P and S waves down to a depth of ~140 km, suggesting that the results obtained for that area are reliable.

[62] The uncertainties in 3-D velocity model are inferred to be ~1% from the checkerboard resolution tests at depths of 25–80 km beneath Kanto. We also evaluated the effect of the Moho depth, which is fixed during the inversions, on the obtained velocity models, by shifting the Moho depth by 3 km deeper and shallower. The results suggested that seismic velocities around the Moho (at depths of 30 and 40 km) can be affected by 1–2%. However, these uncertainties in seismic velocity do not affect our interpretation in this study.

[63] **Acknowledgments.** We would like to thank D. Zhao for providing us with tomographic codes and N. Uchida for providing us with data of small repeating earthquakes. Constructive and careful reviews by D. Okaya, an anonymous reviewer, and an Associate Editor improved the manuscript significantly. We used seismic data from the National Research Institute for Earth Science and Disaster Prevention, Hokkaido University, Hirosaki University, Tohoku University, University of Tokyo, Nagoya University, Kyoto University, Kochi University, Kyushu University, Kagoshima University, the Japan Meteorological Agency, the National Institute of Advanced Industrial Science and Technology, the Geographical Survey Institute, Aomori prefectural government, Tokyo metropolitan government, Shizuoka prefectural government, Kanagawa prefectural government, the City of Yokohama, and the Japan Marine Science and Technology Center. All the figures in this paper are plotted using GMT [*Wessel and Smith*, 1998]. This work was partially supported by a grant from "Global Education and Research Center for Earth and Planetary Dynamics" of Tohoku University Global COE program and the Ministry of Education, Culture, Sports, Science and Technology of Japan.

References

Alt, J. C. (1995), Sulfur isotopic profile through the oceanic crust: Sulfur mobility and seawater-crustal sulfur exchange during hydrothermal alteration, *Geology*, *23*, 585–588, doi:10.1130/0091-7613(1995)023<0585:SIPTTO>2.3.CO;2.

Central Disaster Management Council (2004), Report of the 12th Special Committee on the earthquake just beneath the Tokyo metropolis, Tokyo.

Christensen, N. I. (1996), Poisson's ratio and crustal seismology, *J. Geophys. Res.*, *101*, 3139–3156, doi:10.1029/95JB03446.

Evans, B. W. (1977), Metamorphism of alpine peridotite and serpentinite, *Annu. Rev. Earth Planet. Sci.*, *5*, 397–447, doi:10.1146/annurev.ea.05.050177.002145.

Hacker, B. R., G. A. Abers, and S. M. Peacock (2003), Subduction factory: 1. Theoretical mineralogy, densities, seismic wave speeds, and H_2O contents, *J. Geophys. Res.*, *108*(B1), 2029, doi:10.1029/2001JB001127.

Harada, S. (2004), The precision of recent seismic observation—Observation and data processing by JMA (in Japanese), *Rep. Coord. Comm. Earthquake Predict.*, *71*, 780–783.

Hasegawa, A., and J. Nakajima (2004), Geophysical constraints on slab subduction and arc magmatism, in *The State of the Planet: Frontiers and Challenges in Geophysics*, *Geophys. Monogr. Ser.*, vol. 150, edited by R. S. J. Sparks and C. J. Hawkesworth, pp. 81–94, AGU, Washington, D. C.

Hasegawa, A., J. Nakajima, S. Kita, T. Okada, T. Matsuzawa, and S. Kirby (2007), Anomalous deepening of a belt of intraslab earthquakes in the Pacific slab crust under Kanto, central Japan: Possible anomalous thermal shielding, dehydration reactions, and seismicity caused by shallower cold slab material, *Geophys. Res. Lett.*, *34*, L09305, doi:10.1029/2007GL029616.

Hilairet, N., B. Reynard, Y. Wang, I. Daniel, S. Merkel, N. Nishiyama, and S. Petitgirard (2007), High-pressure creep of serpentine, interseismic deformation, and initiation of subduction, *Science*, *318*, 1910–1913, doi:10.1126/science.1148494.

Hirose, F., J. Nakajima, and A. Hasegawa (2007), Three-dimensional velocity structure in southwestern Japan and configuration of the Philippine Sea slab estimated by double-difference tomography (in Japanese with English abstract), *J. Seismol. Soc. Jpn., Ser. 2*, *60*, 1–20.

Hirose, F., J. Nakajima, and A. Hasegawa (2008a), A three-dimensional velocity structure and configuration of the Philippine Sea slab beneath Kanto district, central Japan, estimated by double-difference tomography (in Japanese with English abstract), *J. Seismol. Soc. Jpn.*, *60*, 123–138.

Hirose, F., J. Nakajima, and A. Hasegawa (2008b), Three-dimensional seismic velocity structure and configuration of the Philippine Sea slab in southwestern Japan estimated by double-difference tomography, *J. Geophys. Res.*, *113*, B09315, doi:10.1029/2007JB005274.

Hori, S. (2006), Seismic activity associated with the subducting motion of the PHS plate beneath the Kanto district, Japan, *Tectonophysics*, *417*, 85–100, doi:10.1016/j.tecto.2005.08.027.

Huchon, P., and P. Labaume (1989), Central Japan triple junction: A three dimensional compression model, *Tectonophysics*, *160*, 117–133, doi:10.1016/0040-1951(89)90387-9.

Hyndman, R., M. Yamano, and D. A. Oleskevich (1997), The seismogenic zone of subduction thrust faults, *Isl. Arc*, *6*, 244–260, doi:10.1111/j.1440-1738.1997.tb00175.x.

Igarashi, T., T. Matsuzawa, N. Umino, and A. Hasegawa (2001), Spatial distribution of focal mechanisms for interplate and intraplate earthquakes associated with the subducting Pacific plate beneath the northeastern Japan arc: A triple-plated deep seismic zone, *J. Geophys. Res.*, *106*, 2177–2191, doi:10.1029/2000JB900386.

Iidaka, T., M. Mizoue, I. Nakamura, T. Tsukuda, K. Sakai, M. Kobayasi, T. Haneda, and S. Hashimoto (1990), The upper boundary of the Philippine sea plate beneath the western Kanto region estimated from S-P-converted wave, *Tectonophysics*, *179*, 321–326, doi:10.1016/0040-1951(90)90297-L.

Ishida, M. (1992), Geometry and relative motion of the Philippine Sea plate and Pacific plate beneath the Kanto-Tokai district, Japan, *J. Geophys. Res.*, *97*, 489–513, doi:10.1029/91JB02567.

Iwamori, H. (2000), Deep subduction of H_2O and deflection of volcanic chain towards backarc near triple junction due to lower temperature, *Earth Planet. Sci. Lett.*, *181*, 41–61, doi:10.1016/S0012-821X(00)00180-1.

Kamimura, A., J. Kasahara, M. Shinohara, R. Hino, H. Shiobara, G. Fujie, and T. Kanazawa (2002), Crustal structure study at the Izu-Bonin subduction zone around 31°N: Implications of serpentinized materials along the subduction plate boundary, *Tectonophysics*, *132*, 105–129.

Kamiya, S., and Y. Kobayashi (2000), Seismological evidence for the existence of serpentinized wedge mantle, *Geophys. Res. Lett.*, *27*, 819–822, doi:10.1029/1999GL011080.

Kamiya, S., and Y. Kobayashi (2007), Thickness variation of the descending Philippine Sea slab and its relationship to volcanism beneath the Kanto-Tokai district, central Japan, *J. Geophys. Res.*, *112*, B06302, doi:10.1029/2005JB004219.

Kimura, H., K. Kasahara, T. Igarashi, and N. Hirata (2006), Repeating earthquake activities associated with the Philippine Sea plate subduction in the Kanto district, central Japan: A new plate configuration revealed by interpolate aseismic slips, *Tectonophysics*, *417*, 101–118, doi:10.1016/j.tecto.2005.06.013.

Kissling, E., W. L. Ellsworth, D. Eberhart-Philiips, and U. Kradolfer (1994), Initial reference models in local earthquakes, *J. Geophys. Res.*, *99*, 19,635–19,646, doi:10.1029/93JB03138.

Kita, S., T. Okada, J. Nakajima, T. Matsuzawa, and A. Hasegawa (2006), Existence of a seismic belt in the upper plane of the double seismic zone extending in the along-arc direction at depths of 70–100 km beneath NE Japan, *Geophys. Res. Lett.*, *33*, L24310, doi:10.1029/2006GL028239.

Kodaira, S., T. Iidaka, A. Kato, J. O. Park, T. Iwasaki, and Y. Kaneda (2004), High pore fluid pressure may cause silent slip in the Nankai trough, *Science*, *304*, 1295–1298, doi:10.1126/science.1096535.

Matsubara, M., H. Hayashi, K. Obara, and K. Kasahara (2005), Low-velocity oceanic crust at the top of the Philippine Sea and Pacific plates beneath the Kanto region, central Japan, imaged by seismic tomography, *J. Geophys. Res.*, *110*, B12304, doi:10.1029/2005JB003673.

Matsubara, M., K. Obara, and K. Kasahara (2008), Three-dimensional P- and S-wave velocity structures beneath the Japan Islands obtained by high-density seismic stations by seismic tomography, *Tectonophysics*, *454*, 86–103, doi:10.1016/j.tecto.2008.04.016.

Moore, D. E., D. A. Lockner, M. Shengli, R. Summers, and J. D. Byerlee (1997), Strength of serpentinite gouges at elevated temperatures, *J. Geophys. Res.*, *102*, 14,787–14,801, doi:10.1029/97JB00995.

Nakajima, J., and A. Hasegawa (2006), Anomalous low-velocity zone and linear alignment of seismicity along it in the subducted Pacific slab beneath Kanto, Japan: Reactivation of subducted fracture zone?, *Geophys. Res. Lett.*, *33*, L16309, doi:10.1029/2006GL026773.

Nakajima, J., and A. Hasegawa (2007), Subduction of the Philippine Sea plate beneath southwestern Japan: Slab geometry and its relationship to arc magmatism, *J. Geophys. Res.*, *112*, B08306, doi:10.1029/2006JB004770.

Nakajima, J., T. Matsuzawa, A. Hasegawa, and D. Zhao (2001), Three-dimensional structure of V_p, V_s, and V_p/V_s beneath northeastern Japan: Implications for arc magmatism and fluids, *J. Geophys. Res.*, *106*, 21,843–21,857, doi:10.1029/2000JB000008.

Nakajima, J., Y. Tsuji, and A. Hasegawa (2009), Seismic evidence for thermally controlled dehydration in subducting oceanic crust, *Geophys. Res. Lett.*, *36*, L03303, doi:10.1029/2008GL036865.

Nakamura, R., K. Satake, S. Toda, T. Uetake, and S. Kamiya (2006), Three-dimensional attenuation (Qs) structure beneath the Kanto district, Japan, as inferred from strong motion records, *Geophys. Res. Lett.*, *33*, L21304, doi:10.1029/2006GL027352.

National Institute for Earth Science and Disaster Prevention (2007), The 2007 Boso SSE event and associated earthquake swarm (in Japanese), *Rep. Coord. Comm. Earthquake Predict.*, *79*, 123–127.

Nishimoto, S., M. Ishikawa, M. Arima, T. Yoshida, and J. Nakajima (2008), Simultaneous high P-T measurements of ultrasonic compressional and shear wave velocities in Ichino-megata mafic xenoliths: Their bearings on seismic velocity perturbations in lower crust of northeast Japan arc, *J. Geophys. Res.*, *113*, B12212, doi:10.1029/2008JB005587.

Nishimura, T., T. Sagiya, and R. Stein (2007), Crustal block kinematics and seismic potential of the northernmost Philippine Sea plate and Izu microplate, central Japan, inferred from GPS and leveling data, *J. Geophys. Res.*, *112*, B05414, doi:10.1029/2005JB004102.

Noguchi, S. (2007), Spatial distribution of seismicity in the subducting Philippine Sea slab and Pacific slab beneath the Kanto district, Japan, and their convergence mode (in Japanese), *Earth Mon.*, *57*, 42–53.

Obara, K. (2002), Nonvolcanic deep tremor associated with subduction in southwest Japan, *Science*, *296*, 1679–1681, doi:10.1126/science.1070378.

Ohmi, S., and S. Hori (2000), Seismic wave conversion near the upper boundary of the Pacific plate beneath the Kanto district, Japan, *Geophys. J. Int.*, *141*, 136–148, doi:10.1046/j.1365-246X.2000.00086.x.

Ohmi, S., and N. Hurukawa (1996), Detection of the subducting crust of oceanic plates beneath the Kanto district, Japan, *Tectonophysics*, *261*, 249–276, doi:10.1016/0040-1951(95)00150-6.

Okada, Y., and K. Kasahara (1990), Earthquake of 1987, off Chiba, central Japan and possible triggering of eastern Tokyo earthquake of 1988, *Tectonophysics*, *172*, 351–364, doi:10.1016/0040-1951(90)90041-6.

Okada, Y., K. Kasahara, S. Hori, K. Obara, S. Sekiguchi, H. Fujiwara, and A. Yamamoto (2004), Recent progress of seismic observation networks in Japan -Hi-net, F-net, K-NET and KiK-net, *Earth Planets Space*, *56*, xv–xviii.

Okino, K., Y. Shimakawa, and S. Nagaoka (1994), Evolution of the Shikoku Basin, *J. Geomagn. Geoelectr.*, *46*, 463–479.

Ozawa, S., S. Miyazaki, Y. Hatanaka, T. Imakiire, M. Kaidzu, and M. Murakimi (2003), Characteristic silent earthquakes in the eastern part of the Boso peninsula, central Japan, *Geophys. Res. Lett.*, *30*(6), 1283, doi:10.1029/2002GL016665.

Ozawa, S., H. Suito, and M. Tobita (2007), Occurrence of quasi-periodic slow-slip off the east coast of the Boso peninsula, central Japan, *Earth Planets Space*, *59*, 1241–1245.

Pacanovsky, K. M., D. Davis, R. Richardson, and D. Coblentz (1999), Intraplate stresses and plate-driving forces in the Philippine Sea Plate, *J. Geophys. Res.*, *104*, 1095–1110, doi:10.1029/98JB02845.

Sato, H., et al. (2005), Earthquake source fault beneath Tokyo, *Science*, *309*, 462–464, doi:10.1126/science.1110489.

Sato, R. (1989), *The Parameter Handbook on Earthquake Faults in Japan*, 390 pp., Kajima Inst., Tokyo.

Schmidt, M. W., and S. Poli (1998), Experimentally based water budgets for dehydrating slabs and consequences for arc magma generation, *Earth Planet. Sci. Lett.*, *163*, 361–379, doi:10.1016/S0012-821X(98)00142-3.

Sekiguchi, S. (2001), A new configuration and a seismic slab of the descending Philippine Sea plate revealed by seismic tomography, *Tectonophysics*, *341*, 19–32, doi:10.1016/S0040-1951(01)00182-2.

Seno, T. (2005), Variation of downdip limit of the seismogenic zone near the Japanese islands: Implications for the serpentinization mechanism of the forearc mantle wedge, *Earth Planet. Sci. Lett.*, *231*, 249–262, doi:10.1016/j.epsl.2004.12.027.

Seno, T. (2007), Verifying the danger of earthquakes occurring directly beneath the metropolitan area: Are earthquakes prone to occur (in Japanese with English abstract), *J. Geogr.*, *132*, 105–129.

Seno, T., and S. Maruyama (1984), Paleogeographic reconstruction and origin of the Philippine Sea plate, *Tectonophysics*, *102*, 53–84, doi:10.1016/0040-1951(84)90008-8.

Seno, T., and T. Takano (1989), Seismotectonics at the trench-trench-trench triple junction off central Honshu, *Pure Appl. Geophys.*, *129*, 27–40, doi:10.1007/BF00874623.

Seno, T., S. Stein, and A. E. Gripp (1993), A model for the motion of the Philippine Sea plate consistent with NUVEL-1 and geological data, *J. Geophys. Res.*, *98*, 17,941–17,948, doi:10.1029/93JB00782.

Seno, T., T. Sakurai, and S. Stein (1996), Can the Okhotsk plate be discriminated from the North American plate?, *J. Geophys. Res.*, *101*, 11,305–11,315, doi:10.1029/96JB00532.

Seno, T., D. Zhao, Y. Kobayashi, and M. Nakamura (2001), Dehydration of serpentinized slab mantle: Seismic evidence from southwest Japan, *Earth Planets Space*, *53*, 861–871.

Soh, W., K. Nakamura, and T. Kimura (1998), Arc-arc collision in the Izu collision zone, central Japan, deduced from the Ashigara Basin and adjacent Tanzawa Mountains, *Isl. Arc*, *7*, 330–341, doi:10.1111/j.1440-1738.1998.00193.x.

Tsuji, Y., J. Nakajima, and A. Hasegawa (2008), Tomographic evidence for hydrated oceanic crust of the Pacific slab beneath northeastern Japan: Implications for water transportation in subduction zones, *Geophys. Res. Lett.*, *35*, L14308, doi:10.1029/2008GL034461.

Uchida, N., A. Hasegawa, J. Nakajima, and T. Matsuzawa (2009), What controls interplate coupling?: Evidence for abrupt change in coupling across a border between two overlying plates in the NE Japan subduction zone, *Earth Planet. Sci. Lett.*, *283*, 111–121, doi:10.1016/j.epsl.2009.04.003.

Ueno, H., S. Hatakeyama, T. Aketagawa, J. Funasaki, and N. Hamada (2002), Improvement of hypocenter determination procedures in the Japan Meteorological Agency (in Japanese), *Q. J. Seismol.*, *65*, 123–134.

Ulmer, P., and V. Trommsdorff (1995), Serpentine stability to mantle depths and subduction-related magmatism, *Science*, *268*, 858–861, doi:10.1126/science.268.5212.858.

Wada, I., K. Wang, J. He, and R. D. Hyndman (2008), Weakening of the subduction interface and its effects on surface heat flow, slab dehydration, and mantle wedge serpentinization, *J. Geophys. Res.*, *113*, B04402, doi:10.1029/2007JB005190.

Wald, D. J., and P. G. Somerville (1995), Variable-slip rupture model of the great 1923 Kanto, Japan earthquake: Geodetic and body-waveform analysis, *Bull. Seismol. Soc. Am.*, *85*, 159–177.

Wessel, P., and W. H. F. Smith (1998), New, improved version of the Generic Mapping Tools released, *Eos Trans. AGU*, *79*, 579, doi:10.1029/98EO00426.

Wu, F., D. Okaya, H. Sato, and N. Hirata (2007), Interaction between two subducting plates under Tokyo and its possible effects on seismic hazards, *Geophys. Res. Lett.*, *34*, L18301, doi:10.1029/2007GL030763.

Zhao, D., A. Hasegawa, and S. Horiuchi (1992a), Tomographic imaging of P and S wave velocity structure beneath northeastern Japan, *J. Geophys. Res.*, *97*, 19,909–19,928, doi:10.1029/92JB00603.

Zhao, D., S. Horiuchi, and A. Hasegawa (1992b), Seismic velocity structure of the crust beneath the Japan Islands, *Tectonophysics*, *212*, 289–301, doi:10.1016/0040-1951(92)90296-I.

A. Hasegawa and J. Nakajima, Research Center for Prediction of Earthquakes and Volcanic Eruptions, Graduate School of Science, Tohoku University, Sendai 980-8578, Japan. (nakajima@aob.geophys.tohoku.ac.jp)

F. Hirose, Seismology and Volcanology Research Department, Meteorological Research Institute, Nagamine 1-1, Tsukuba 305-0052, Japan.